Food Research International 204 (2025) 115916

Contents lists available at ScienceDirect

Food Research International

journal homepage: www.elsevier.com/locate/foodres

Encapsulated hesperetin modulates inflammatory responses in an *in vitro* intestinal immune co-culture model

Xiangnan Meng [a,*], Monic M.M. Tomassen [b], Christos Fryganas [a], Vincenzo Fogliano [a], Tamara Hoppenbrouwers [a,b]

[a] Food Quality and Design, Wageningen University & Research, P.O. Box 17, 6700 AA Wageningen, the Netherlands
[b] Wageningen Food & Biobased Research, Wageningen University & Research, Stippeneng 4, 6708 WE Wageningen, the Netherlands

ARTICLE INFO

Keywords:
Caco-2
THP-1
Co-culture
Hesperetin
Nanoliposomes
Anti-inflammatory
Metabolomics

ABSTRACT

In vitro cell models are an effective way to evaluate the biological activities of functional compounds. Hesperetin (HST) is a flavanone with various potential health-related benefits, and encapsulation improved its stability and bioavailability. This study aimed to investigate the anti-inflammatory effects of encapsulated HST using different delivery systems, including β-cyclodextrin (CD), nanoliposomes (NL), and NL coated with chitosan (CH) and carrageenan (CGN). A Caco-2 and THP-1 co-culture model characterized by direct cell-to-cell contact was developed, and these delivery systems were digested *in vitro* and subsequently tested on this model. The addition of lipopolysaccharide (LPS) in the model resulted in high secretion of the pro-inflammatory cytokines (IL-8, TNF-α, and IL-1β), the upregulation of the phenotype genes (CD68 and CD80) and the inflammation-related genes (MYD88, NFκB, and COX-2), marking the differentiation of M0 macrophages into M1 macrophages. Among the delivery systems, HST encapsulated in CH and CGN coated NL (CGN-CH-NL-HST) was the most effective in suppressing the production of IL-8 and expression of MYD88 and COX-2 in the inflammatory co-culture model. Metabolomic data showed that the M1 macrophage metabolic profile was changed by applying free HST and encapsulated HST, mostly in glycolysis and amino acid metabolism. Encapsulated HST in the CGN-CH-NL delivery system showed anti-inflammatory activity in the Caco-2 and THP-1 direct co-culture model, suggesting a potential of encapsulated bioactive compounds in treating inflammatory bowel disease.

1. Introduction

The intestine is a complex organ in the human body. Its functions include nutrient absorption, immune surveillance, and the symbiotic relationship with microbiota is a pivotal factor regulating the overall health (Hickey et al., 2023). Disruption of its homeostasis may lead to intestinal inflammation: 2.5–3 million individuals (0.4 %) in Europe are suffering from inflammatory bowel disease (IBD), and data indicate it is even becoming more prevalent (Kumar et al., 2023).

2D *in vitro* cell models are simple, cost-effective, and standardized tools to mimic the human intestine (Fedi et al., 2021). The Caco-2 cell line is widely used in intestinal cell models as it can differentiate into enterocyte-like cells with tight junctions and microvilli, thereby resembling the intestinal epithelial layer. Beside the epithelial layer, the intestine contains the largest number of immune cells compared to any other organ in the human body and therefore, the immune cell should also be included in intestinal cell models (Gu, Kim, & Yun, 2021). It is suggested that the 2D Transwell model can allow the interaction between the intestinal epithelium and underlying immune cell populations (Roh, Chen, Rudolph, Gee, & Kaplan, 2021).

The 2D Transwell model is composed of a plate with inserts, which can separate, by the insert membrane, into two compartments, namely the apical and basolateral sides. In mimicking intestinal immunity, the Caco-2 cells are usually seeded apically, whereas macrophages are seeded basolaterally. THP-1 monocytes are often used, as they can differentiate into macrophage-like cells, exhibiting phagocytic activity, cytokine production, and inflammatory responses (Protić-Rosić, Lopandić, Popović, Blagojević, & Gavrović-Jankulović, 2024). Co-culture models combining Caco-2 and THP-1 cells in a 2D Transwell system provide an approximation of the intestinal tissue physiology, thereby facilitating research into intestinal immunity (Paul et al., 2023). However, the interaction between Caco-2 and THP-1 cells in the conventional model system is indirect due to the insert in the Transwell, and the basolateral dilution effect further reduces the amount of metabolite

* Corresponding author at: Wageningen University & Research, Food Quality and Design, Axis X1116, P.O. Box 17, 6700 AA Wageningen, the Netherlands.
E-mail address: xiangnan.meng@wur.nl (X. Meng).

https://doi.org/10.1016/j.foodres.2025.115916
Received 25 October 2024; Received in revised form 14 January 2025; Accepted 2 February 2025
Available online 3 February 2025

transmission. In previous research, Caco-2 cells and primary cells have been directly co-cultured to study the effect of particle size of rice-derived arabinoxylan fibers on innate immune training and resilience (Moerings et al., 2024). In this study, we co-cultured Caco-2 cells in direct contact with THP-1 macrophages and stimulated the model to mimic intestinal inflammation.

The bioprocess of inflammation is complex, including the activation of different signaling pathways to regulate genes and produce pro-inflammatory cytokines. Lipopolysaccharide (LPS) has been conventionally used to study inflammation, due to the abundance of inflammatory effects that it generates through Toll-like receptor 4 (TLR4) signaling (Tucureanu et al., 2018). When TLR4 is activated, downstream genes related to inflammation are also activated, such as MYD88 and NFκB. Some pro-inflammatory cytokines like TNF-α, IL-8, IL-1β, and IL-18 are frequently elevated in inflammation (Liu et al., 2021). Cyclooxygenase-2 (COX-2), a key enzyme in the mediation of inflammation, is one of the genes that can also be induced by NFκB during early response by inflammatory cytokines (Oliveira et al., 2024). To alleviate and prevent intestinal inflammation, much research is dedicated to finding drugs or bioactives with strong anti-inflammatory capacities.

Natural flavonoids have been considered a promising anti-inflammatory family (Hasnat, Shompa, Islam, Alam, Richi, Emon, Ashrafi, Ahmed, Chowdhury, Fatema, Hossain, Ghosh, & Ahmed, 2024). Hesperetin (HST), a flavanone commonly found in the peels of citrus fruits like oranges and lemons, has shown anti-inflammatory potential. For example, HST was found to alleviate the p-NFκB/Iba-1/TNF-α expression in murine microglia cells stimulated with LPS (Muhammad, Ikram, Ullah, Rehman, & Kim, 2019), and HST also reduced the LPS-stimulated gene expression of IL-1β, IL-6, TNF-α, iNOS, and COX-2 in mouse mammary epithelial cells (Ran et al., 2024). However, HST shares the common problem of flavonoids of limited oral bioavailability (Mariano, Li, Singh, McClements, & Davidov-Pardo, 2024). To address this issue, our previous research suggested that encapsulating the flavanone hesperetin in cyclodextrin (CD-HST), in nanoliposomes (NL-HST), and in carrageenan and chitosan-coated nanoliposomes (CGN-CH-NL-HST) improved its bioavailability and enhanced HST absorption in the Caco-2 cell monolayer (Meng, Fryganas, Fogliano, & Hoppenbrouwers, 2024).

In this study, we aimed to investigate the anti-inflammatory effects of encapsulated HST using a Caco-2 and THP-1 direct co-culture model. Cytokines, inflammation-related gene expression, and cell metabolites were analyzed to evaluate the effectiveness of the free and encapsulated HST against intestinal inflammation.

2. Materials and methods

2.1. Materials

Hesperetin, L-α-lecithin from soybean, cholesterol from sheep wool, Triton X-100, chitosan (75–85 % deacetylated, 50 kDa-190 kDa), λ-carrageenan, maltodextrin, β-cyclodextrin, bile salt, pepsin (3100 U/mg) from pig gastric mucosa, and pancreatin from porcine pancreas (p1750-500G lot: SLBT7088, lipase activity: 342 U/mg, trypsin activity: 3.13U/mg, α-amylase activity: 68 U/mg), acetic acid, acetonitrile, methanol, ethanol, phosphate buffered saline (PBS), fetal bovine serum (FBS), 3-(4,5-dimethylthiazol-2-yl)-2,5-diphenyltetrazolium bromide (MTT), dimethyl sulfoxide (DMSO), formic acid, penicillin, phorbol 12-myristate 13-acetate (PMA), streptomycin, and lipopolysaccharide (LPS) were all from Sigma-Aldrich (St. Louis, USA). Caco-2 cells and THP-1 monocytes were supplied from American Type Culture Collection (Manassas, USA). Dulbecco's modified Eagle's medium (DMEM), DMEM without phenol red, RPMI 1640 medium with HEPES and GlutaMAX™ Supplement, RPMI 1640 medium without phenol red, TRIzol™ Reagent, SYBR Safe DNA gel stain were from Thermo Fisher Scientific Inc. (Waltham, USA). 96-well plates (3595, Corning Incorporated, USA), 24-well Transwell plates 662,640, 12-well plates 665,180 and 12-well Transwell plates 665,640 from Greiner bio-one (Kremsmünster, Austria), 7-Aminoactinomycin D (7-AAD) from BD Pharmingen (559925, New Jersey, USA), iQ™ SYBR Green supermix from Bio-Rad Laboratories (California, USA), Milli-Q water from Purelab® Flex, Veolia Ecosystem S.A (Aubervilliers, France).

2.2. Sample preparation

Delivery systems of encapsulated HST, CD-HST, NL-HST, and CGN-CH-NL-HST were prepared as described previously (Meng et al., 2024). Briefly, CD-HST was freeze dried in a 1:1 mol ratio of β-CD: HST in Milli-Q water, NL-HST was prepared by thin-film hydration combined with probe sonication, while 0.6 %wt CH and 0.5 %wt CGN were used to coat NL-HST and form CGN-CH-NL-HST. The amount of HST in delivery systems was determined by HPLC-UV/Vis analysis, and the encapsulation efficiency was calculated by our previous study (Meng et al., 2024). Briefly, 20 μL of the sample was injected into a Polaris C18 column (4.6 × 150 mm, 5 μm, Varian, Inc, Netherlands). The column temperature was set at 40 °C set and 47.5 % acetonitrile mixed with 0.1 % formic acid in Milli-Q was used as a mobile phase. The flow rate was 1.0 mL/min in the system and HST was detected at a wavelength of 286.3 nm.

The delivery systems, free HST, and Milli-Q water (as digestion control) were digested following the INFOGEST procedure as reported previously (Brodkorb et al., 2019; Meng et al., 2024). Briefly, the initial concentration of HST before digestion was 90 μg/mL in all samples. A total of 10 mL of samples were digested in the simulated gastric fluid (pH = 3.0) with the 2000 U/mL final activity of pepsin for 2 h, following 2-hour digestion in simulated intestinal fluid (pH = 7.0) with 10 mmol/L bile salts, and the 2000 U/mL final lipase activity in pancreatin. The final digested samples were snap-frozen using liquid nitrogen and stored at −80 °C until further use.

2.3. Cell culture

2.3.1. Caco-2 cell culture

Caco-2 cells from passages 30 to 40 were cultured and maintained in DMEM containing 10 % v/v FBS in 75 cm^2 plastic flasks. A volume of 150 μL cells at a concentration of 0.225 × 10^6 cells/ml were seeded apically at each insert in 24-well Transwell plates, and 750 μL medium was added to the basolateral side of inserts. The cells were cultivated at 37 °C and 5 % CO_2 in humidified air for 21 days to differentiate into small intestinal-like cells. The culture medium was refreshed every two days.

2.3.2. THP-1 cell culture

THP-1 cells under passage 25 were cultured and maintained in RPMI 1640 containing 10 % v/v FBS and 1 % v/v penicillin and streptomycin in 75 cm^2 plastic flasks. For the single THP-1 macrophages, each well of a 12-well plate was seeded with 1 mL of cells at a concentration of 1 × 10^6 cells/mL in the presence of 100 ng/mL PMA. After 48 h, cells were washed twice with culture medium and rested for 5 days (Hoppenbrouwers et al., 2022). The medium with 1 μg/mL LPS was added and incubated for 24 h to induce M1 differentiation, which is the most common macrophage phenotype in low-grade intestinal inflammation levels (Luzardo-Ocampo, Loarca-Piña, & Gonzalez de Mejia, 2020).

2.3.3. Co-culture experimental design and LPS inflammation activation

The direct co-culture is able to better mimic the intestine immune response by direct cell touch and less dilution in the basolateral side. A general diagram of the co-culture experimental design is presented in Fig. 1. Inserts containing Caco-2 and THP-1 monocytes were obtained following the culturing methods described in sections (2.3.1. Caco-2 cell culture and 2.3.2. THP-1 cell culture). THP-1 monocytes (300 μL of 1 × 10^6 cells/mL) were seeded into the insert with 100 ng/mL PMA in 12-well Transwell plates. A total of 1500 μL medium with 100 ng/mL

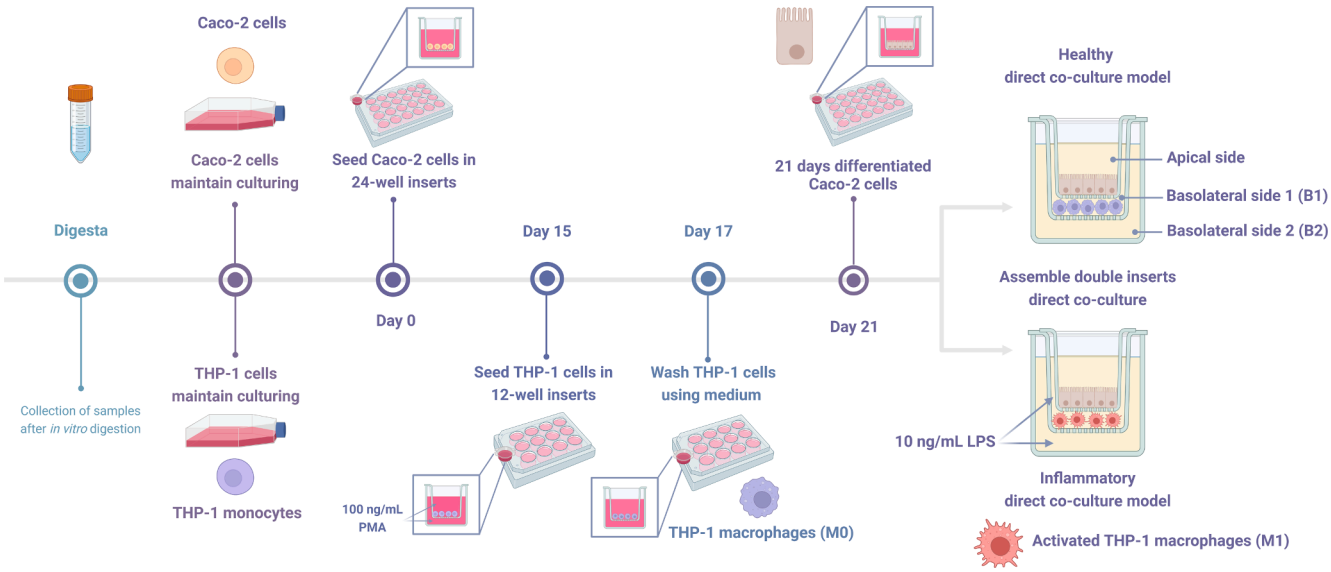

Fig. 1. Experimental design for the direct co-culture model. Created using BioRender.

PMA was also added to the basolateral side of inserts. After 48 h, cells were washed twice with culture medium and rested for 3 days.

On the experimental day, the 24-well Caco-2 inserts were assembled onto the 12-well THP-1 inserts. A volume of 150 μL samples were added apically, and 300 μL and 1500 μL of RPMI 1640 (without phenol red and FBS, with 1 % v/v penicillin and streptomycin) were added to compartments B1 and B2, respectively. In the inflammatory model, a final concentration of 10 ng/mL LPS was added to the B1 and B2 compartments.

2.3.4. Sample treatment and cell medium collection

To investigate the direct effects of the encapsulated systems on THP-1 macrophages, 1 mL of different concentrations of free HST (0–90 μg/mL), non-digested samples (containing 5.6 μg/mL HST, confirmed by the cytotoxicity from the 7-AAD assay in 2.3.5. Cytotoxicity assessment), and basolateral Caco-2 cell medium treated by digested samples were added to the single THP-1M1 macrophages. The medium was collected after 24 h incubation and stored at −80 ℃.

The 150 μL of 8x diluted digested samples (digestion control, free HST, CD-HST, NL-HST, and CGN-CH-NL-HST) were added apically to either the single Caco-2 cell monolayer for 2 h or to the direct co-culture models (healthy and inflammatory) for 6 h. Our previous study has confirmed that this dilution factor had no cytotoxicity (Meng et al., 2024). The basolateral medium was collected and stored at −80 ℃ for further use.

2.3.5. Cytotoxicity assessment

In the single Caco-2 monolayer, based on our previous research, the largest amount of HST was transported after 2 h of incubation (Meng et al., 2024). Therefore, an MTT assay was performed to evaluate the cytotoxicity of digested samples after 2 h. In this procedure, 100 μL of MTT solution (0.5 mg/mL) was added to Caco-2 cells for 2 h, and the formed formazan precipitate in each insert was subsequently dissolved in 150 μL dimethyl sulfoxide and shaken for 5 min. The absorbance of the formazan product was measured at 570 nm with a microplate reader (Tecan Infinite M200, Tecan Group Ltd., Switzerland).

To investigate the cytotoxicity of pure HST and basolateral Caco-2 medium samples in the single THP-1 M1 macrophage, a 7-AAD assay was applied. Cells were collected by adding 0.25 % trypsin and stained with 1 % of 7-AAD in the dark for 30 min at 4 ℃. The fluorescent signal of dead cells was determined using a flow cytometer (CytoFLEX, Beckman Coulter, Inc., USA).

2.3.6. Transepithelial electrical resistance (TEER)

TEER was measured using an electrical resistance system (Millicell ERS-2 Volt-Ohm Meter, Millipore Amsterdam, Netherlands). The TEER was measured and marked as Tpre to ensure barrier integrity before adding samples and assembling co-culture systems, which should be higher than 650 Ohm for 24-well Transwell plates. The TEER was also measured at 0, 1, 2, 4, and 6 h after adding samples, and its value should be higher than 400 Ohm for the 12-well inserts in the co-culture system.

2.4. Evaluation of the impact of encapsulated HST and free HST on the modulation of inflammatory parameters in monocultures and co-cultures

2.4.1. Cytokines production

All cytokines (human IL-8, TNF-α, IL-1β, IL-18, and IL-10) were measured by ELISA according to the manufacturer's protocol. IL-8, TNF-α, IL-1β, and IL-10 were measured by ELISA MAX™ Deluxe Set (BioLegend, Koblenz, Germany). IL-18 was measured by the Human Total IL-18 ELISA Kit (Proteintech Group, Inc. Manchester, UK). The absorbance of the specific enzyme-substrate reaction used in the ELISA assay was detected by a Tecan Infinite 200PRO (Tecan, Männedorf, Switzerland).

2.4.2. RNA extraction and cDNA synthesis

In the co-culture model, both Caco-2 and THP-1 macrophages were lysed using 175 μL TRIzol in each insert. RNA was extracted and purified followed by an RNeasy kit (Qiagen, Venlo, the Netherlands) including a DNase digestion (RNase-Free DNase Set, Qiagen, Venlo, the Netherlands) according to the manufacturer's protocol. The integrity of the ribosomal RNA was verified through 1 % agarose gel electrophoresis (Eurogentec, Liège, Belgium). RNA concentration and purity were checked by the Nanodrop spectrophotometer system (Nanodrop Technologies, Wilmington, USA), and 200 ng RNA with a ratio (Abs 260/280 nm) between 1.8 and 2.1 were selected to synthesize cDNA using iScript cDNA synthesis kit (Bio-Rad, Veenendaal, the Netherlands) in each reaction. cDNA was stored at −20 ℃ for further analysis.

2.4.3. Expression analysis of inflammatory genes

Quantitative real-time PCR (qPCR) was performed to analyze gene expression. Primer sequences and sources were listed in Table S1 (Abreu et al., 2002; Chanput, Mes, Vreeburg, Savelkoul, & Wichers, 2010; Vreeburg, Bastiaan-Net, & Mes, 2011; Liu, 2024) and were synthesized by Biolegio (Nijmegen, the Netherlands). To check primer efficiency, a series of dilution ratios (1x, 10x, 100x, 1000x, 10000x) of 5 μL cDNA and

Milli-Q (blank) were mixed with 10 μL iQ™ SYBR Green supermix, and 2.5 μL of forward and reverse primers, to a total volume of 20 μL. Amplifications were carried on a CFX96 Touch Real-Time PCR Detection System (Bio-Rad Laboratories, California, USA), and the thermal cycling conditions: 95 °C for 3 min; 39 cycles of 95 °C for 10 s, 60 °C for 30 s. The specificity of each pair of primers was checked by melting curve analysis (95 °C for 10 s, 65 °C for 5 min, and a continuous raise in temperature to 95 °C at 0.5 °C/s ramp rate followed by 95 °C for 5 s). The PCR products were checked by electrophoresis on 2 % agarose gels stained with SYBR safe to make sure that there was no formation of primer dimers. The primers with PCR efficiency values (E) between 90 % and 150 % and R^2 of standard curves higher than 0.98 were selected.

The stability test was performed by qbase$^+$ software (v3.4, Biogazelle, Gent, Belgium), and RPLP0 and β-actin were selected as housekeeping genes (geNorm M value < 1.5 and coefficient of variation < 0.5) (Sarker et al., 2018). The gene relative quantities of all samples were normalized to geometric means of reference genes RPLP0 and β-actin expression (ΔCT) and medium-stimulated cells via the ΔΔCT method using the qbase$^+$ default settings.

2.5. Untargeted metabolomics of direct co-culture medium

2.5.1. Liquid chromatography quadrupole time-of-flight mass spectrometry (LC-qTOF-MS)

To study the change in metabolism of the co-culture model before and after inflammation and the effects of the samples, non-targeted metabolite analysis was performed by using a Nexera XS UPLC system (Shimadzu Corporation, Kyoto, Japan) coupled with an LCMS-9030 quadrupole time-of-flight mass spectrometer (Shimadzu Corporation, Kyoto, Japan). The UPLC unit consisted of a SIL-40CX3 autosampler, an LC-40D XS solvent delivery pump, a DGU-405 degassing unit, a CTO-40S column oven, and a CBM-40 lite system controller. The qTOF-MS system was equipped with a standard electrospray ionization (ESI) source unit and a calibrant delivery system (CDS). The medium (5 μL) was injected into an Acquity UPLC BEH C18 column (1.7 μm, 2.1 × 100 mm, Waters Corporation, Netherlands) with an Acquity UPLC BEH C18 VanGuard Pre-column (130 Å, 1.7 μm, 2.1 mm × 5 mm, Waters Corporation, Netherlands) and a SeQuant® ZIC®-HILIC column (200 Å, 3.5 μm, 4.6 × 150 mm, Merck KGaA, Darmstadt, Germany) with a SeQuant® ZIC®-HILIC™ pre-column (5 μm, 2.1 × 20 mm, Merck KGaA, Darmstadt, Germany) to analyze compounds with different polarity to capture the full overview of HST and amino acid metabolites by cells during inflammation.

For medium polar compounds, the flow rate was set at 0.3 mL/min and the column temperature at 40 °C. The mobile phases consisted of 0.1 % formic acid (solvent A), acetonitrile with 0.1 % formic acid (solvent B) with the following elution profile: 90 % A to 10 % A (0–14 min), 10 % A (14–16 min), 90 % A (16–18 min). MS data was collected with ion accumulation (ID off) for 18 mins. External mass calibration was performed by using ESI-L Low Concentration Tuning Mix 100 mL (Agilent Technologies, Amstelveen, Netherlands). Both positive and negative ionization modes were used for the MS analysis. The voltage of the ion-spray ionization was 4.5 kV and −3.5 kV for ESI+ and ESI−, respectively. For both positive and negative ionization, the temperature of the electrospray ionization probe, desolvation line, and heat block were set at 300 °C, 250 °C, and 400 °C, respectively. At the same time, the flow rates of the drying gas and heating gas were both set at 10 mL/min, and the flow rate of the nebulizer gas was 2 mL/min. The CID energy ramp was set at 35 ± 15 eV for the positive mode, and 35.0 ± 17.0 eV for the negative mode, and the pressure of CID gas followed the tuning file, the charge states were set between 1 and 3. For data-dependent acquisition (DDA) analysis of two modes, the number of DDA events was set to 20 with a total loop time of 1.1 s and 19 with a total loop time of 1.0 s, MS1 and MS2 were acquired over an m/z range of 50–1000 Da, and the event time for the full scan was set at 0.1 s, whereas for each DDA each event was set at 0.05 s. The precursor intensity threshold was 1000.

For polar compounds, the flow rate was set at 0.7 mL/min, The mobile phases consisted of 0.1 % formic acid (solvent A), acetonitrile with 0.1 % formic acid (solvent B), and 10 mM NH_4HCOO (solvent C) with the following elution profile: for whole 22 min, solvent C was stable (2 %), 8 % A (0–3 min), 8 % A to 28 % A (3–5 min), 28 % A to 78 % A (5–11 min), 78 % A (11–17 min), 78 % A to 8 % A (17–19 min), 8 % A (19–22 min). MS data was collected with ion accumulation (ID off) for 22 mins. The CID energy ramp was set at 35.0 ± 17.0 eV for positive mode, and 35.0 ± 17.0 for negative mode. The precursor intensity threshold was 1000 for the positive mode and 3000 for the negative mode, respectively. Other parameters were the same with medium polar compounds analysis.

2.5.2. Metabolite data processing

The collected MS data (.lcd file) was processed using the MS-DIAL software (version 4.9.221218, RIKEN Center for Sustainable Resource Science: Metabolome Informatics Research Team, Kanagawa, Japan). Automatic peak finding and LOWESS normalization were performed as reported before (Meng et al., 2024). The identification was carried out by comparing MS1, MS2, and retention time with the database from authentic standards (https://systemsomicslab.github.io/compms/msdial/main.html#MSP, lasted visited on 03-10-2024).

MetaboAnalyst 6.0 (https://www.metaboanalyst.ca/) was used for statistical and integrative analysis of metabolomics data (Pang et al., 2022). Principal components analysis (PCA) and partial least squares discriminant analysis (PLSDA) were performed to achieve dimensionality reduction of metabolites in the healthy co-culture model and inflammatory co-culture model. A volcano plot was used to select significant compounds to distinguish the healthy and inflammatory co-culture models (Abuawad, Mbadugha, Ghaemmaghami, & Kim, 2020). Heatmap clustering was used to display the key compounds and their relevance. Before visualization, the peak area was normalized by log 10 transformation (Meng et al., 2024).

2.6. Statistical analysis

The results were presented as mean ± standard error of the mean (SEM) unless additional state (n = 3). Fig. 1 was created using BioRender.com. GraphPad Prism 10.1.2 (GraphPad Software, La Jolla, CA) was used to represent the results graphically, one-way analysis of variance (ANOVA) followed with Dunnett's multiple comparisons tests to compare multiple treatments to a single control group ($P < 0.05$), and one-way analysis of variance (ANOVA) followed with Tukey's multiple comparisons tests to compare all groups ($P < 0.05$).

3. Results

3.1. Sample treatments on cytotoxicity in the different models

Fig. S1A shows an optimal TEER value (higher than 650 Ohm) during 2 h incubation in the single Caco-2 cell monolayer, and Fig. S1B presents the absorbance compared with medium control showed that the Caco-2 cell activity was not hindered. Fig. S2A, B, and C report that the single THP-1 M1 macrophage cell viability was not affected by different concentrations of HST (up to 90 μg/mL), non-digested samples, and the collected basolateral medium from the single Caco-2 cell monolayer after *in vitro* digestion, respectively.

Fig. S3A and B show the TEER value measured in the co-culture models: it remained higher than 400 Ohm in both healthy and inflammatory models, which is still a good value indicating a fully functioning cell layer. Thus, the Caco-2 and THP-1 direct co-culture model maintained intact barrier function after 6 h.

3.2. Sample treatments on cytokines secretion in the single THP-1M1 macrophages

The cytokines IL-8 and TNF-α are typical indicators of the degree of inflammation induced by LPS. A series of different concentrations of free HST were applied to 24-hour LPS-stimulated single THP-1 M1 macrophages to investigate its potential to mitigate inflammation. Fig. 2A shows untreated M1 macrophages (medium control) produced the highest amount of IL-8, and HST treatments decreased the production of IL-8 in a dose-dependent manner. Control experiments reported in Fig. S4A showed that HST did not affect the secretion of TNF-α by M1 macrophages.

Some non-digested/non-absorbed compounds in the gut can also contact immune cells under the intestinal epithelium as macrophages can extend their pseudopodia through the gaps between epithelial cells and capture antigens directly (Coombes & Powrie, 2008). Fig. 2B indicates that all non-digested samples after encapsulation could also markedly decrease the production of IL-8 ($P < 0.05$) compared to the medium control group, while only the non-digested samples of free HST and CGN-CH-NL-HST increased the TNF-α secretion compared to the medium control ($P < 0.01$) as reported in Fig. S4B.

3.3. Secretion of TNF-α and IL-8 by THP-1 macrophages after the samples transit through the intestinal epithelium

To investigate the effects of digested encapsulated HST samples after intestinal epithelial absorption on pro-inflammatory cytokines secretion, THP-1 M1 macrophages were exposed to the basolateral medium of Caco-2 cells which were treated with digested samples. Fig. 2C represents the results of secretion of IL-8 after 24 h exposure. IL-8 secretion level was significantly lower in all tested groups ($P < 0.0001$) compared to the medium control. Incubating with untreated Caco-2 basolateral medium (DMEM group) also showed low IL-8 secretion which might indicate immunomodulating effects of the intestinal barrier to inflamed M1 macrophages. Basolateral medium from digested CGN-CH-NL-HST was the most effective in decreasing IL-8 production compared to both the medium control and the digestion control groups ($P < 0.05$). Free HST, CD-HST, and NL-HST encapsulation systems did not reduce IL-8 secretion compared to the digestion control. Similarly to IL-8, the secretion of TNF-α was also reduced by the untreated Caco-2 basolateral medium (DMEM group) ($P < 0.0001$). In line with the effects of HST on TNF-α production by THP-1 M1 macrophages (see Fig. S4A), the digested encapsulated HST samples in the basolateral Caco-2 medium did not affect TNF-α secretion ($P > 0.05$), as shown in Fig. 2D.

To better mimic the physiological intestinal conditions, Caco-2 cells and THP-1 cells were cultured in a double-transwell system to allow cell-to-cell contact. Fig. 3 depicts IL-8 and TNF-α contents in the medium after the co-culture system was treated by the digested samples for 6 h, and models stimulated without or with LPS in the medium were marked as the healthy and inflammatory model, respectively. In Fig. 3A, there were no significant differences in IL-8 secretion between treatments in the healthy model. In Fig. 3B, treatments also did not influence the TNF-α production compared with digestion control in the healthy model. These results showed that digested samples would not trigger inflammation when the co-culture model was in "healthy" status.

Fig. 3C and D highlight that both IL-8 and TNF-α secretion increased

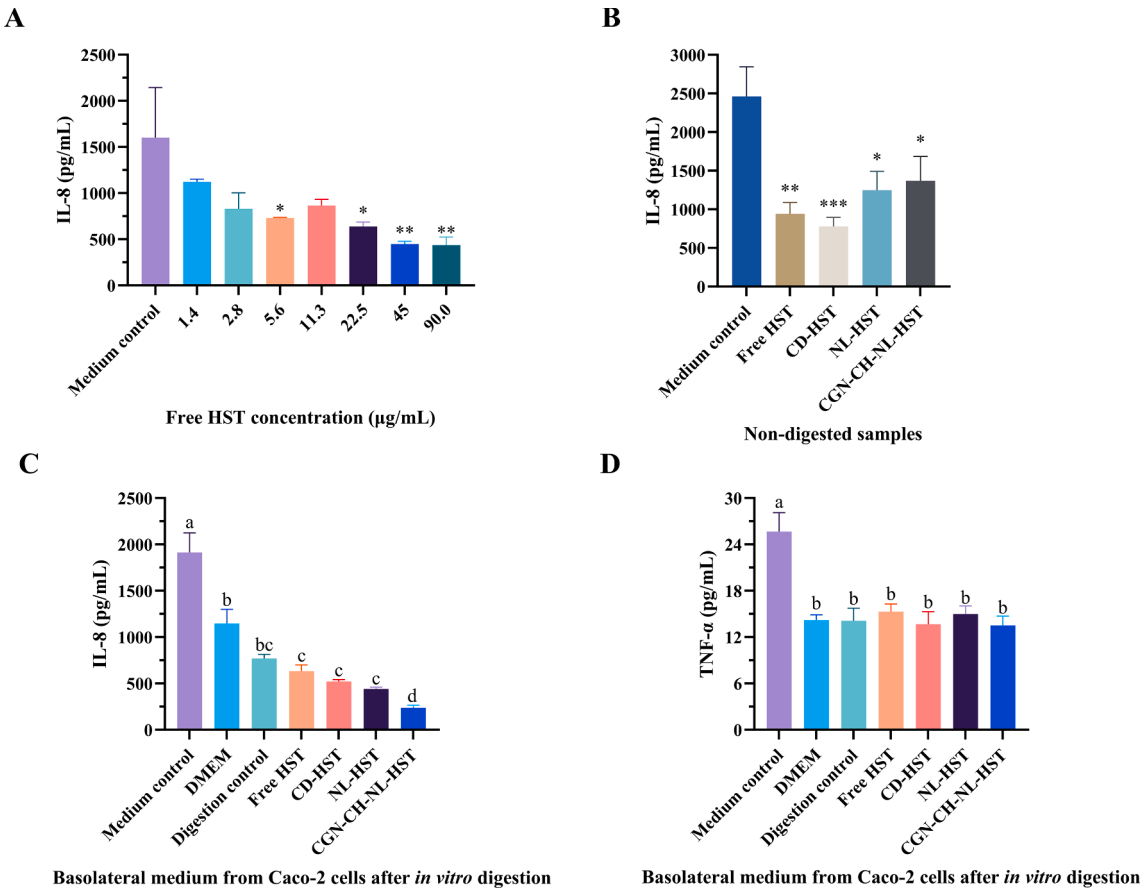

Fig. 2. IL-8 and TNF-α secretion in the single THP-1M1 macrophages. (A) IL-8 secretion of different concentrations of HST treatments; (B) IL-8 secretion of treatments of non-digested Free HST, CD-HST, NL-HST, and CGN-CH-NL-HST. Compared to the medium control group, $^{*}P < 0.05$, $^{**}P < 0.01$, $^{***}P < 0.001$. (C) IL-8 secretion in the single THP-1M1 macrophages treated by basolateral medium from Caco-2 cells; (D) TNF-α secretion in the single THP-1M1 macrophages treated by basolateral medium from Caco-2 cells. In Figure C and D, bars labeled with different lowercase letters are significantly different between treatments ($P < 0.05$).

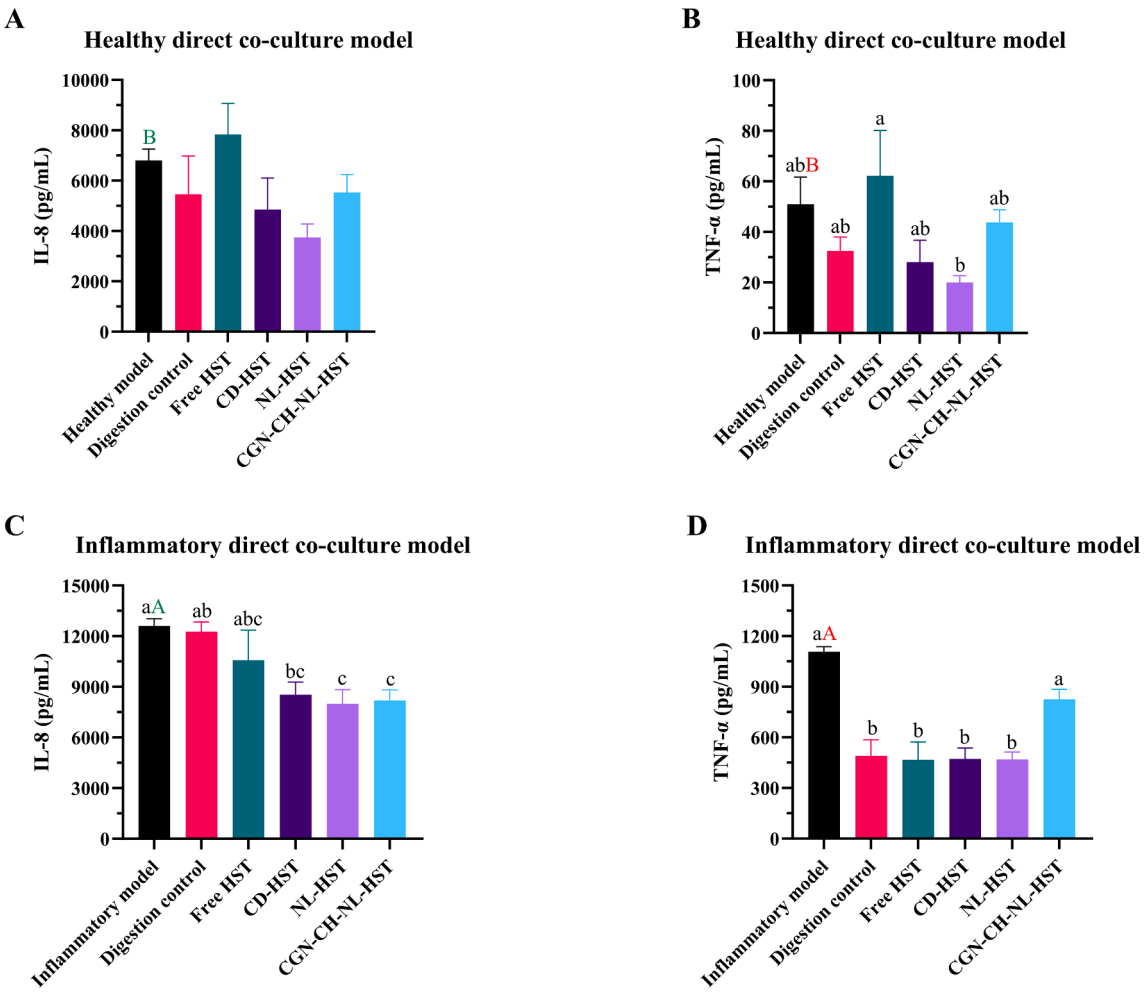

Fig. 3. IL-8 and TNF-α secretion in the healthy (A and B) and inflammatory (C and D) direct co-culture models when treated with digested samples, the bars named healthy model and inflammatory model are the medium-treated control group. Bars labeled with different lowercase letters differ significantly between samples in the same model ($P < 0.05$). Green capital letters labeled the significant difference in IL-8 production between the healthy and inflammatory models ($P < 0.05$), and red capital letters labeled the significant difference in TNF-α production between the healthy and inflammatory models ($P < 0.05$).

significantly when initiating inflammation in the co-culture model by adding LPS. IL-8 increased from 6803.5 pg/mL to 12588.9 pg/mL, and TNF-α increased from 50.9 pg/mL to 1107.4 pg/mL, suggesting successful inflammation of the model. In the treatment of the inflammatory co-culture model, Fig. 3C shows the digestion control and free HST did not reduce IL-8 secretion compared to the inflammatory model ($P > 0.05$). NL-HST and CGN-CH-NL-HST were able to significantly reduce IL-8 secretion compared to digestion control ($P < 0.05$). Fig. 3C also presents that treating the inflammation with CD-HST showed that IL-8 secretion was not significantly different in comparison to the digestion control, although it showed a noticeable difference when compared to the untreated inflammatory model ($P < 0.05$). Fig. 3D shows the digestion control could reduce TNF-α secretion compared to the untreated inflammatory model ($P < 0.0001$), suggesting enzymes and bile salts in the medium digesta could influence TNF-α production, while digested CGN-CH-NL-HST cannot decrease TNF-α production compared to the digestion control. The reason could be that the 6-hour point is not the optimal window to detect the potential reducing effect of CGN-CH-NL-HST on TNF-α, as TNF-α production kinetics could differ from those of IL-8. In line with the previous findings (Fig. 2D), none of the other treatments were able to affect TNF-α secretion compared to digestion control ($P > 0.05$), as presented in Fig. 3D. IL-1β results in Fig. S5 also showed a significant difference in the healthy model and inflammatory model ($P < 0.0001$), while all treatments were not able to decrease its secretion compared with the digestion control. The results of IL-18 and IL-10 were not present in this article because they were lower than the detection limitation.

3.4. *Differences in transcriptional regulation of inflammatory genes*

The effect of the digested samples on phenotype and inflammatory gene expression was further investigated in the direct co-culture models. The gene expression of the inflammatory direct co-culture model was tested first. Compared to the healthy co-culture model, Fig. 4B, D, E and F show significantly increased expression of CD80, MyD88, NFκB, and COX-2 in THP-1 macrophages of the inflammatory co-culture model, respectively. This indicates the inflammatory co-culture model effectively elicited M1 inflammatory properties. Fig. 5C and D indicate that NOX1 was also significantly upregulated in the inflammatory co-culture model compared to the healthy co-culture model ($P < 0.01$), which suggests that LPS could cause oxidation stress in Caco-2 cells.

In Fig. 4, the effect of the various HST samples on the expression of CD68 and CD80 genes, which are important markers of THP-1 cell differentiation into M1 macrophages, is reported. As shown in Fig. 4A, CD68 was expressed more in the inflammatory model compared to the healthy model, but none of the samples changed the levels of CD68 expression in the healthy model ($P > 0.05$), CD80 is specifically associated with the M1 macrophage phenotype, playing a pro-inflammatory and immune-stimulating role. Similar to the CD68 expression, Fig. 4B shows that digested samples did not change the CD80 expression

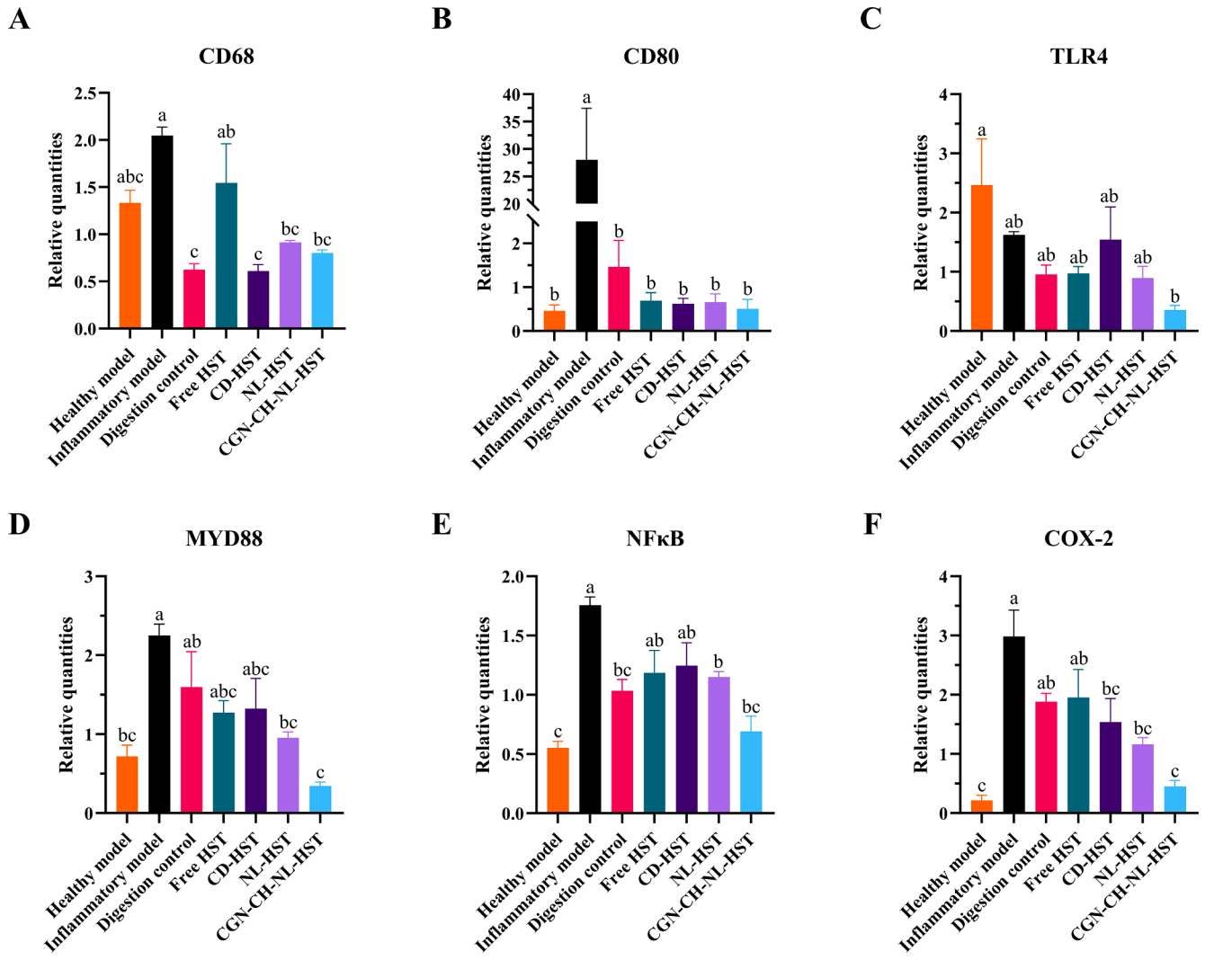

Fig. 4. Gene regulation of THP-1 macrophages in the healthy and inflammatory Caco-2 and THP-1 direct co-culture models, the bars marked healthy and inflammatory model are the medium control of the healthy and inflammatory models, respectively. Relative quantities of selected genes were normalized to the average expression of the endogenous reference genes RPLP0 and β-actin. (A) CD68 and (B) CD80 are related to M1 phenotype, the samples were applied in the THP-1 M0 macrophages in the healthy co-culture model to check the changes in phenotypes. Inflammation-related genes of THP-1 M1 macrophages in the inflammatory Caco-2 and THP-1 direct co-culture model: (C) TLR4, (D) MYD88, (E) NFκB, and (F) COX-2. The samples were applied in the THP-1 M1 macrophages in the inflammatory co-culture model to check the anti-inflammatory effects. Bars labeled with different lowercase letters differ significantly between treatments for the same gene transcription ($P < 0.05$).

compared to the healthy model ($P > 0.05$). These data showed that digested samples did not affect the phenotype of M0 in the healthy model.

TLR4 expression is shown in Fig. 4C, which is a receptor to recognize LPS, its expression was low in the inflammatory co-culture model compared to the healthy model and remained unaffected by the other treatments ($P > 0.05$). This might indicate that the negative feedback phase was predominating at the 6-hour point, in which the expression of TLR4 was downregulated after initial activation by LPS (Soares, Pimentel-Nunes, Roncon-Albuquerque, & Leite-Moreira, 2010). CGN-CH-NL-HST further decreased the TLR4 expression compared with the healthy model. In contrast, CGN-CH-NL-HST had a higher secretion of TNF-α in Fig. 3D, suggesting other alternative pathways (TLR2, TLR3 and other TLRs) and the downstream pathways (NFκB) still were active to produce TNF-α. As shown in the inflammatory model in Fig. 4D, when TLR4 is activated, the MYD88 adapter protein helps to activate NFκB and produce pro-inflammatory cytokines, especially in M1 macrophages. MYD88 was significantly downregulated following CGN-CH-NL-HST treatment compared to the digestion control ($P < 0.01$) in the inflammatory model, whereas none of the other treatments showed this effect ($P > 0.05$). Fig. 4E shows that NL-HST and CGN-CH-NL-HST significantly reduced NFκB expression compared to the untreated inflammatory model. However, no treatments affected NFκB expression compared to the digestion control, but its expression was reduced by the digestion control compared to the inflammatory model, indicating that the digestive enzymes impacted the expression of NFκB more than the treatments. COX-2 expression reported in Fig. 4F indicated its expression was significantly reduced by CGN-CH-NL-HST compared to the digestion control and free HST ($P < 0.05$).

Some key genes can reflect the barrier integrity of the Caco-2 monolayer in the co-culture model. MLCK activation is critical for the regulation of tight junctions, which are structures that maintain the integrity of the epithelial barrier. Fig. 5A and B indicate no significant difference in the expression of MLCK between the healthy and inflammatory models, meaning that intestinal tight junction permeability was stable. In Fig. 5A, the digestion control significantly increased the MLCK expression compared to the healthy model, but the other digested samples (free HST, CD-HST, and CGN-CH-NL-HST) significantly reduced

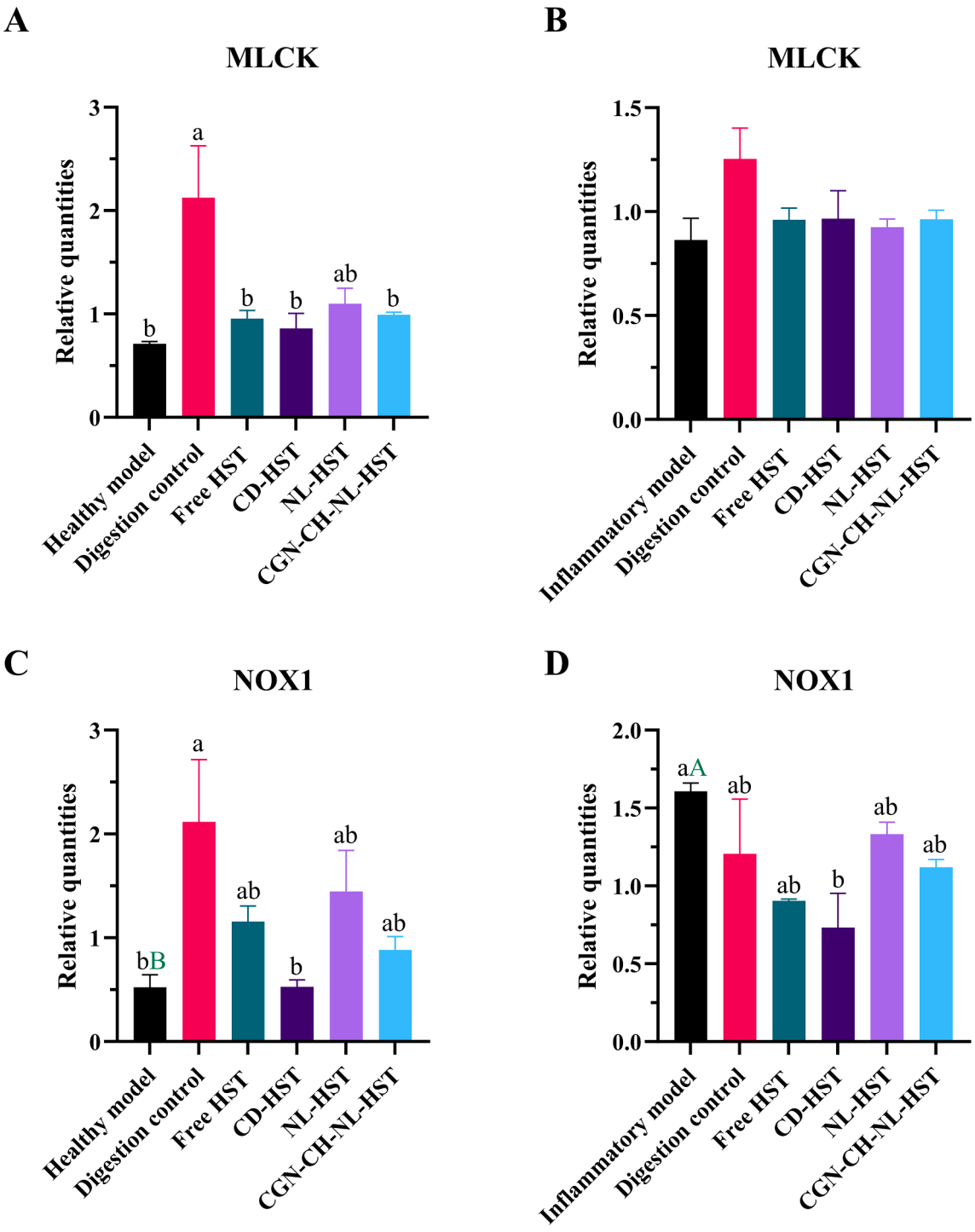

Fig. 5. Gene regulation of barrier function of Caco-2 cells in the healthy and inflammatory direct co-culture model when treated with digested samples, the bars named healthy model and inflammatory model are the medium-treated control group. MLCK is related to the epithelial barrier, MLCK expression in the healthy co-culture model (A) and inflammatory co-culture model (B). NOX1 is the major NADPH oxidase expressed in the gut, NOX1 expression in the healthy co-culture model (C) and inflammatory co-culture model (D). Bars labeled with different lowercase letters differ significantly between treatments ($P < 0.05$) for the same gene transcription. Green capital letters labeled the significant difference in NOX1 transcription between the healthy and inflammatory models ($P < 0.05$).

the expression of MLCK to the level of the healthy model compared with digestion control ($P < 0.05$). In Fig. 5B, the treatments did not affect MLCK expression level compared to the digestion control in the inflammatory model. All treatments did not change the MLCK expression in the two models providing further evidence that direct-contacted macrophages do not affect barrier integrity at the transcriptional level. This stable status of the barrier was also proved by TEER and cytotoxicity results, reported in Fig. S1.

NOX1 can code an enzyme that produces reactive oxygen species (ROS) by transferring electrons from NADPH to oxygen. During inflammation, the expression of NOX1 will be increased, leading to more ROS production, while NOX1-mediated ROS production can also promote inflammatory responses. Fig. 5C shows the expression of NOX1 was increased with the addition of digestion control compared with the healthy model ($P < 0.01$), while other digested samples reduced the increase in NOX1 transcript levels induced by the digested control,

especially CD-HST ($P < 0.05$). These treatments could probably relieve possible oxidation stress caused by digestion control (enzymes and bile salts) in the healthy model. As shown in Fig. 5D, LPS-induced NOX1 overexpression was predominant in the inflammatory direct co-culture model because digestion control did not increase the NOX1 expression. There were also no significant differences in NOX1 expression among the treatments compared to the digestion control. Similarly, Fig. S6A shows that NFκB expression levels did not significantly differ between samples in the inflammatory co-culture model ($P > 0.05$).

3.5. The comparison of metabolic profiles of healthy and inflammatory models

Untargeted metabolomics analysis was performed to investigate the variability of cell metabolites under different models and treatments. As shown in Fig. S7, a total of 109 metabolites were identified in this study. More specifically the metabolic profile consisted of 20 amino acids and derivatives, 13 carboxylic acids and derivatives, 11 phenols and polyphenols, 10 carbohydrates and derivatives, 9 organic acids,7 flavonoids and derivatives, 7 lipids and fatty acids, 6 steroids and terpenoids, 4 alkaloids, 3 peptides and proteins, 2 nucleotides and nucleosides, and 17 undefined compounds.

Multivariable statistical analysis was employed to analyze the metabolomics data, aiming to gain a deeper understanding of the metabolic changes in the healthy co-culture model and the inflammatory co-culture model. The PLSDA results presented in Fig. 6A showed a good cluster in the healthy co-culture model and a significant separation between the two models with 95 % confidential ellipses. The first two principal components explained 40.8 % and 8.1 % of the total variation, indicating a clear shift in the cell metabolites induced by the treatment. The smaller, more circular green ellipses indicated less variance within the treatments in the healthy model, while the elongated pink ellipses suggested greater variance and potential outliers within the treatments in the inflammatory model.

A volcano plot was generated to verify the significant differences in metabolites. In Fig. 6B the x-axis represented the magnitude of change in the inflammatory co-culture model/healthy co-culture model. The distribution of metabolite points was around the y-axis, with 50 points standing out in the top left and right quadrants, and the top 10 significant points were marked names. The size of the points was larger and the colors were darker (red or blue) indicating greater significance ($P < 0.05$) and bigger fold change (>2). 15 points in the top right quadrant with log2 (fold change) > 1 and −log10 (p-value) > 1.3 ($P < 0.05$) represented metabolites significantly upregulated in the inflammatory co-culture model group (such as sucrose, 2-acetamidophenol, histidine, and allothreonine, etc.), while 45 points in the top left quadrant with log2 fold change < -1 and −log10 p-value > 1.3 ($P < 0.05$) were metabolites significantly downregulated in the inflammatory co-culture model group (5-hydroxyindole-3-acetic acid, cysteic acid, D-fructose, aspartic acid, glutamic acid, and L-tyrosine, etc.). The grey points near the origin (59 points) with low fold changes and high p-values did not show significant differences and were not of primary interest.

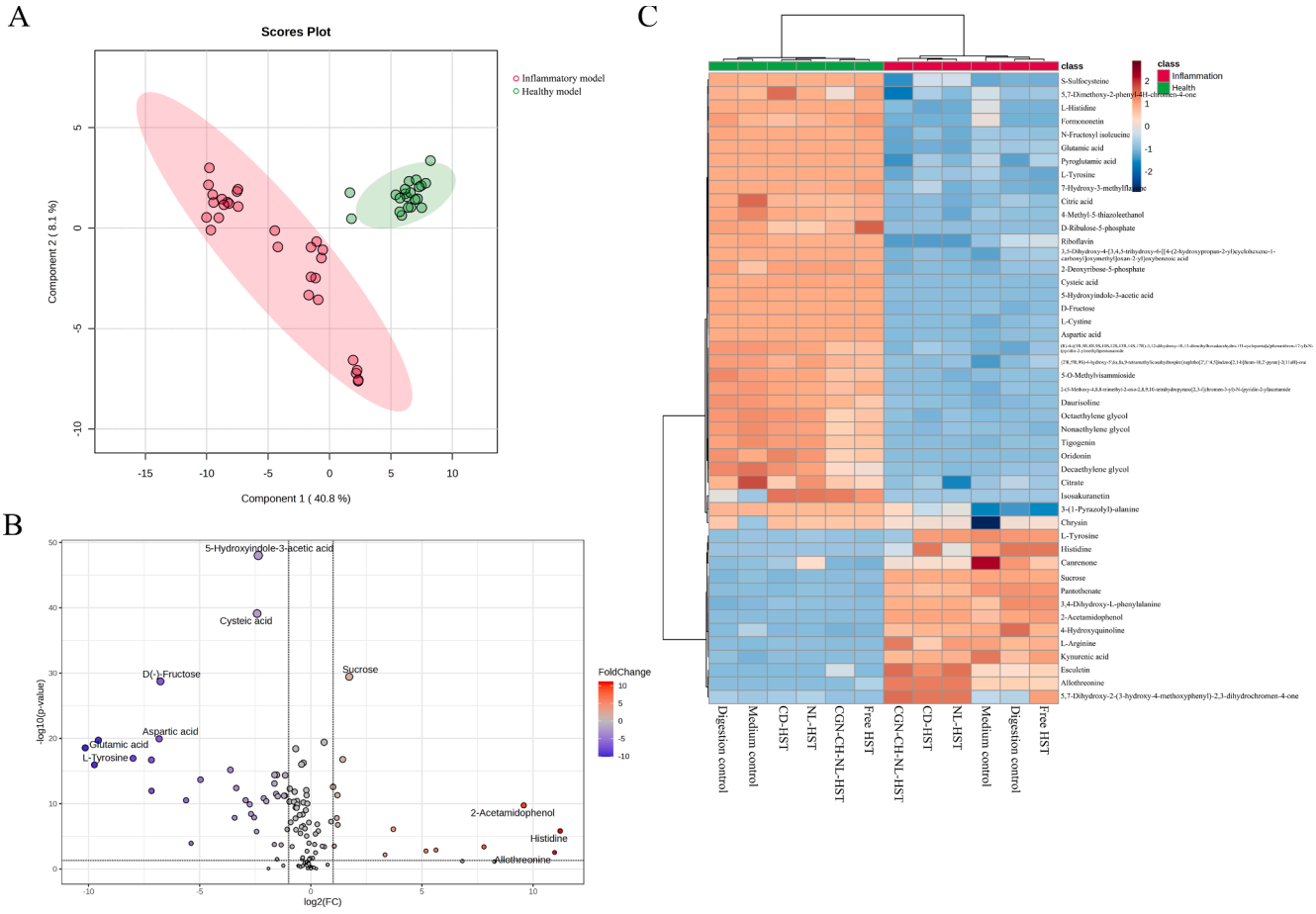

Fig. 6. Multivariate statistical analysis of metabolites from healthy and inflammatory co-culture model. (A) A plot of PLSDA score, different colored ellipses represent 95 % confidence intervals; (B) A volcano plot, fold change in the inflammatory/healthy model, metabolites dots with color show significant changes ($P < 0.05$), and blue means downregulation, red means upregulation; (C) A hierarchical heatmap clustering analysis (HCA) of significant metabolites in the volcano plot shows differences in metabolites in and between groups. The relative abundance of distinct substances was shown on a color-coded scale from red to blue, moving from high to low.

The 47 metabolites showing significant variation from the volcano plot were presented in the clustering heatmap of Fig. 6C to investigate the possible trends in different treatments in the same model. Three missing points were filtered out when the data was normalized. The heatmap shows distinct patterns with 13 metabolites having high production (red) and 34 metabolites having low production (blue) in the inflammatory co-culture model. The treatment groups of the inflammatory model differed in the colors of several of the same metabolites, such as citrate, 3-(1-pyrazolyl)-alanine, chrysin, L-tyrosine, histidine, canrenone, pantothenate, 2-acetamidophenol, 4-hydroxyquinoline, indicating that the different treatments affected the production of metabolites. Compared with the medium control in the inflammatory model, the synthesis of these metabolites was potentially changed to the healthy model after treatment. The production of L-tyrosine, histidine, canrenone, pantothenate, and 4-hydroxyquinoline was decreased after treatment with CGN-CH-NL-HST compared to the digestion control, which possibly was related to the anti-inflammatory properties of the sample.

Several key metabolites in the heatmap of Fig. 6C showed differences between different treatments in the inflammatory co-culture model, therefore a PLSDA was performed to show the overview of all metabolites under inflammatory conditions. The results reported in Fig. 7A indicated that the digestion control and CGN-CH-NL-HST could be distinguished from the other three groups, the first two principal components interpreted 17.7 % and 31.9 % of the total variation, indicating the variability of cell metabolites. However, the 95 % confidence ellipses of free HST, CD-HST, and NL-HST were overlapping in Fig. 7A, suggesting that their metabolites were quite similar. To assess the anti-inflammatory ability of CD-HST, NL-HST, and CGN-CH-NL-HST, they were examined separately with these two controls because the digestion control was a digested blank control and free HST was a non-encapsulated HST control, and the results are shown in Fig. 7B, C, and D, respectively. Each figure contained three distinct ellipses. In CD-HST (Fig. 7B), component 1 explained 7.1 % of the variation, and component 2 accounted for 24.1 % of the variation, the total was 31.2 %. In NL-HST (Fig. 7C), component 1 occupied 39.1 % of variation, and component 2 was 15.3 %, for a total of 54.4 %. In CGN-CH-NL-HST (Fig. 7D), component 1 interpreted 32.1 % of the variation, and component 2 explained 22.9 %, for a total of 55.0 %. Fig. 7C and D might be a stronger plot given the higher variation explained.

The clustering heatmap in Fig. 8 was generated to highlight the metabolites with high VIP scores (>1), indicating their strong influence in differentiating the groups. Based on the amounts of metabolites in the treatment groups, four clusters could be distinguished. In cluster 1, CD-HST, NL-HST, and CGN-CH-ML-HST had the highest amount of metabolites compared to digestion control and free HST. In cluster 2, three treatments (CD-HST, NL-HST, and CGN-CH-NL-HST) and free HST raised the amount of metabolites compared to the digestion control. In cluster 3, opposite to cluster 2, three treatments (CD-HST, NL-HST, and CGN-CH-NL-HST) and free HST decreased the amount of metabolites compared to the digestion control. In cluster 4, CD-HST, NL-HST, and CGN-CH-ML-HST present the lowest amount of metabolites compared to free HST and digestion control.

The metabolites in the same cluster were quite different in chemical properties, but the metabolites in clusters (cluster 1 and 2) with a higher amount than the digestion control could have possible anti-inflammatory properties because the digestion control was the most inflamed of all treatments. Cluster 2 showed the same metabolic pattern,

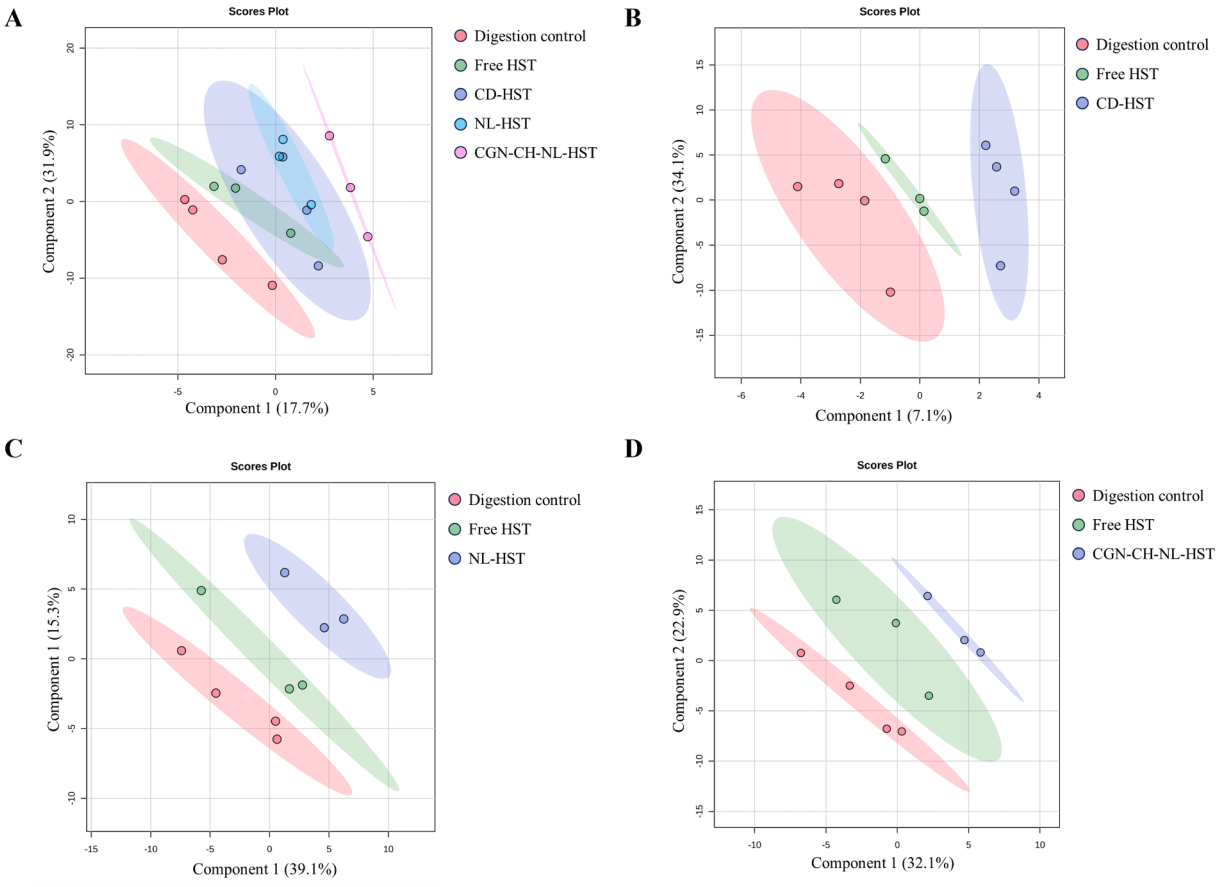

Fig. 7. PLSDA of metabolites in the inflammatory co-culture model under different treatments, each dot represents one biological replicate, and different colored ellipses represent 95% confidence intervals. (A) All identified metabolites in all groups; (B) Digestion control, free HST, and CD-HST; (C) Digestion control, free HST, and NL-HST; (D) Digestion control, free HST, and CGN-CH-NL-HST.

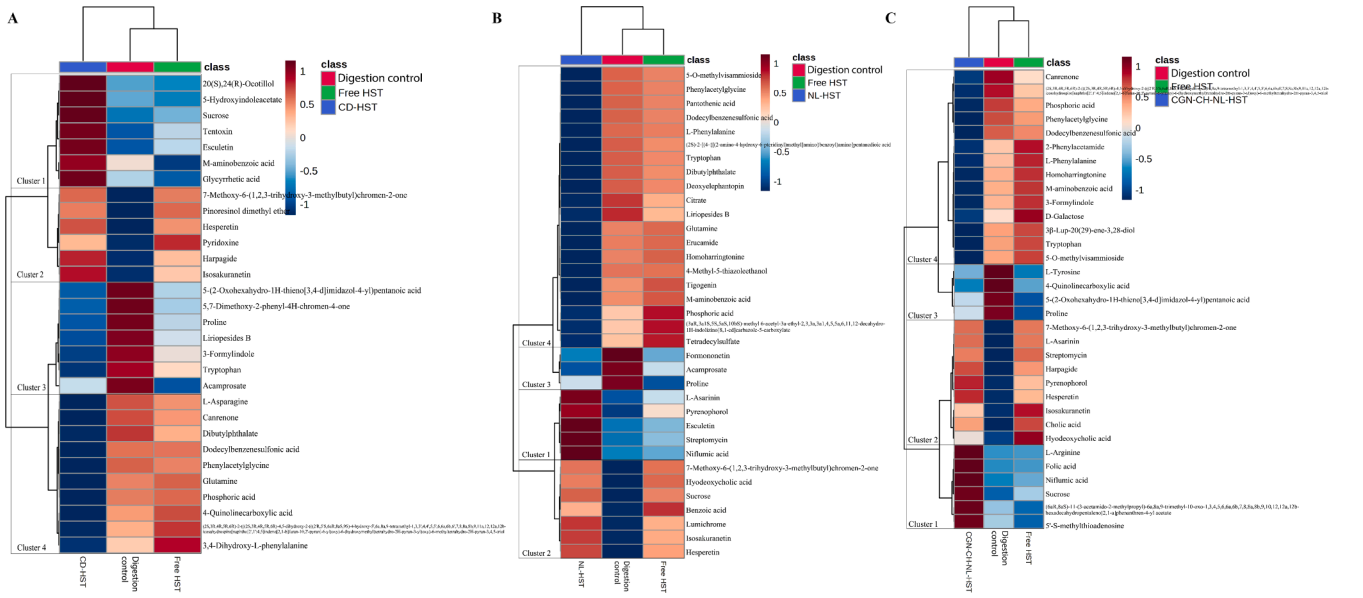

Fig. 8. Clustering heatmaps of VIP > 1 compounds. (A) Digestion control, free HST, and CD-HST; (B) Digestion control, free HST, and NL-HST; (C) Digestion control, free HST, and CGN-CH-NL-HST.

which was the treatments and free HST both had higher amounts of metabolites than the digestion control group, and HST belonged to these clusters, indicating that those metabolites were related to hesperetin, including 7-methoxy-6-(1,2,3-trihydroxy-3-methylbutyl) chromen-2-one, pinoresinol dimethyl ether, pyridoxine, harpagide, isosakuranetin, hyodeoxycholic acid, sucrose, benzoic acid, lumichrome, L-asarinin, streptomycin, pyrenophorol, and cholic acid.

4. Discussion

Intestinal *in vitro* cell models are frequently used to screen the potential functionality of substances to improve human health. In this study, the existing Caco-2 and THP-1 co-culture model was improved by allowing cell-to-cell contact. This model was fully functioning as shown by the ability to mimic an inflammatory phenotype after stimulation with LPS, as indicated by the increase in IL-8, TNF-α, and IL-1β secretion, enhanced CD80, NFκB, MYD88, and COX-2 gene expression and metabolic alterations. Our data showed that HST could reduce intestinal inflammation especially when it was encapsulated in a nanoliposome system coated with chitosan and carrageenan.

To test the functionality of bioactives in intestinal cell models, their bioavailability after oral administration should be considered. The Caco-2 and THP-1 direct co-culture model is a good way to mimic gut immune and it is more physiologically relevant because the THP-1 cells are just underneath Caco-2 cells, shortening the distance between the two cells, reducing the impact of the dilution effect caused by the diffusion in the basolateral side, making cytokines and other chemicals more effective. Moreover, if THP-1 cells and Caco-2 cells are in direct contact or are situated very close to each other can be connected by gap junctions. Juxtacrine signaling facilitates the easy passage of signaling molecules to adjacent cells across these junctions. This implies that several cells can react to a signal received by a single cell, promoting cell-to-cell crosstalk. In this study, the Caco-2 and THP-1 direct co-culture model was specifically designed to investigate intestinal immune effects of compounds after gastric and intestinal digestion.

The production of IL-8 decreased as the concentration of HST increased in the single THP-1 M1 macrophages in our study, suggesting that HST could be useful in easing inflammation. Research showed neutrophils and recently recruited macrophages are responsible for the production of IL-8 in IBD patients (Grimm, Pavli, Doe, Grimm, & F Doe, 1996). IL-8 is a powerful neutrophil chemoattractant and increased in inflamed mucosa, indicating that it is an effective cytokine to study the anti-inflammatory action of HST in our model intestine.

In this study, the non-digested original samples were also tested in the THP-1 M1 macrophages because the immune cells can interact with unabsorbed parts in the digestive gut. The non-digested samples contained the same amount of HST in total, but the CGN-CH-NL-HST showed a less pronounced IL-8 lowering effect than the free HST. This could be because the encapsulated HST was protected by the CGN-CH-NL, making it unlikely to interact with inflammatory cells and exhibit IL-8-reducing activity. Similar findings were observed in the study of antioxidant of encapsulated neohesperidin in pectin and chitosan-coated nanoliposomes, where non-digested capsules showed lower antioxidant activity compared to free neohesperidin. (Shishir et al., 2019). For non-digested NL-HST and CGN-CH-NL-HST samples, observed decreases in IL-8 production in the single THP-1M1 macrophages may be due to the carrier components (e.g., phospholipids, carrageenan, or chitosan). Non-digested CD-HST samples showed a similar influence with free HST in a decrease of IL-8 in the single THP-1M1 macrophages. This could result from the hydrophilic outer surface of CD improved the solubility of CD-HST, but the stability of the complex could be influenced by the medium matrix, causing the release of HST.

These interesting data revealed the potential of HST in mitigating LPS-induced inflammation, but absorption/intestinal function should be taken into account, as well as cross-talk between the cell types. First, to assess the anti-inflammatory effects of absorbed substances without direct cell-to-cell contact between the epithelium and immune cells, the basolateral medium was collected from the single Caco-2 cell monolayer and applied to the THP-1 M1 macrophages after *in vitro* digestion. It was noticeable that the basolateral Caco-2 medium alone significantly reduced the IL-8 secretion. Compared to THP-1 M1 macrophages, the LPS-stimulated THP-1 and Caco-2 co-culture model showed a considerably lower induction of cytokine release, and additional data showed that the presence of Caco-2 cells inhibited the macrophage-driven stress response. Looking at other basolateral medium from digested samples, only CGN-CH-NL-HST could significantly decrease the IL-8 production than other groups compared to the digestion control, the reason could be more HST was absorbed into the basolateral medium (Meng et al., 2024), thereby executing anti-inflammatory effects. This indicated that more complex cell models are far more resilient than a single cell culturing, and only the absorbed portion of bioactives should be considered functional when targeting intestinal inflammation.

Therefore, developing multi-cell co-culture *in vitro* models increases the ability to mimic the absorption and functionality of bioactives *in vivo*.

In the inflammatory direct co-culture model (Fig. 3), low anti-inflammatory activity of free HST could be associated with its poor bioavailability. NL-HST and CGN-CH-NL-HST had the most effective suppression of IL-8 secretion. This is probably because these encapsulation systems promoted the transportation of HST over the epithelial barrier. One reason is that the encapsulation system protected HST from harsh environments during digestion, preventing its degradation and resulting in more HST reaching to the epithelial barrier. More available HST for the intestinal cell could cause more transported HST across the epithelial layer. The other is that lysophospholipids will be generated after phospholipid hydrolysis by phospholipase and bile salts, which can form micelles with polyphenols to enhance cellular uptake of polyphenols. These may be advantages of NL-based encapsulation systems for the intestine-targeted delivery as we also showed in our previous paper (Meng et al., 2024). HST was the bioactive compound in this study, and different concentrations of free HST showed anti-inflammatory effects (Fig. 2A). To limit the size of the biological testing, the empty capsules were not tested, which is a limitation of the study. We assumed the wall materials of encapsulations (polysaccharides) would not have significant biological activities on the THP-1 cells underlying the Caco-2 monolayer because they cannot be digested. Many studies have examined the anti-inflammatory effects of encapsulated bioactives in different models. The focus was mainly on the ability of encapsulation to increase resistance to oral and gastric digestion of bioactives while on the way to reaching the intestine, particularly for those that are poorly soluble in water or easily broken down in the gastrointestinal tract. For instance, zein-pectin core/shell nanoparticles were a highly effective delivery system for resveratrol, as they significantly increased its bioavailability and inhibited NO, PGE2, IL-1β, IL-6, and TNF-α, while promoting IL-10 release in RAW 264.7 cells (Y. Liu et al., 2020). Curcumin and emodin encapsulated in chitosan and trehalose cross-linked hydrogel could achieve controlled drug release in the colon and decrease TNF-α and IL-6 expression in RAW 264.7 cells and mice (Lei et al., 2023).

Regulation of inflammation-related genes and their signaling pathways play a key role in immune response and disease progression. In human dental pulp stem cells, the LPS-mediated transcriptional and post-translational up-regulated IL-8, which was a process that also involves TLR4, MYD88, NFκB, and MAPK (He et al., 2013). In this study, TLR4/MYD88/NFκB was relevant in CGN-CH-NL-HST treatment because MYD88 was significantly inhibited, and the other two genes had downregulated trends (not significant) compared to the digestion control. The reason could be 6 h was not the optimal time to detect changes in TLR4 and NFκB. MYD88 is an essential adapter for TLR-transmitted signaling pathways inducing proinflammatory cytokines. LPS activated Human intrahepatic biliary epithelial cells via a TLR4-MYD88-dependent pathway, increasing the IL-8 secretion (Yokoyama et al., 2006). Rosmarinic acid effectively attenuated LPS-induced mastitis in mice by inhibiting the TLR4/MYD88/NFκB signaling pathway (Jiang et al., 2018).

Oxidative stress and inflammatory responses are interconnected. Significant suppression of expressed COX-2 was observed when the inflammatory Caco-2 and THP-1 direct co-culture model was exposed to CGN-CH-NL-HST. This phenomenon is consistent with other studies on the anti-inflammatory effects of polyphenolic compounds. Polyphenols derived from lentil hulls were reported to have the ability to lower COX-2 and iNOS production in an inflammatory Caco-2 and RAW 264.7 co-culture model (Peng et al., 2022). The expression of COX-2 was also reduced by bound polyphenols found in the insoluble dietary fiber of navel orange peel in an inflammatory Caco-2 and RAW264.7 co-culture model (Chang et al., 2024). The attenuation of oxidative stress markers could complement the suppression of inflammatory pathways, creating a synergistic effect in reducing inflammation. The decrease in IL-8, MYD88, and COX-2 suggested that CGN-CH-NL-HST may target key inflammatory mediators and prevent oxidation. The modulation of IL-8 only may not reflect the mediation of all pro-inflammatory cytokines, and the qPCR alone is not strong enough to support the signaling pathway because high mRNA levels do not always correlate with high protein levels due to post-transcriptional and post-translational modifications (Koussounadis, Langdon, Um, Harrison, & Smith, 2015). To overcome this limitation, it is recommended to measure more related cytokines and genes, and the downstream protein in the future.

In our study, the significant metabolites between healthy and inflammatory models were identified by untargeted metabolomics analysis. Most of the differences in the metabolite profiles observed between the healthy and inflammatory co-culture models are not easy to explain. Thus, several key metabolites were selected to discuss their relationship with macrophage inflammation, including citrate, 2-deoxyribose-5-phosphate, D-ribulose 5-phosphate, and L-arginine. The function and polarization of macrophages are closely related to metabolic changes. M1 macrophages are characterized by enhanced glycolysis, high level of glutathione, increased expression of ferritin, elevated expression of COX-2, low expression of COX-1, augmented activity of inducible nitric oxide synthase (iNOS) 2, and decreased activity of arginase 1 (Arg1) (Li, Yang, Xiong, Jiang, Wang, & Li, 2023). Our data showed citrate was reduced in the inflamed model, and this was also reported before (Mendes, Gaspar, Conde, Mano, & Duarte, 2019). One reason could be that activated macrophages are essentially glycolytic cells to produce ATP, and the activity of the citric acid cycle was suppressed in M1 cells compared to other cell types, then the production of citrate was decreased. Another reason could be citrate was redirected to other pathways. For instance, considering the expression of COX-2 was upregulated in M1 cells (Fig. 4F), citrate can be exported from the mitochondria to the cytoplasm and converted into acetyl-CoA by ATP citrate lyase (ACLY). Acetyl-CoA is a key precursor for the synthesis of fatty acids and subsequently arachidonic acid, and arachidonic acid is a substrate for COX-2. Therefore, increased COX-2 activity requires higher citrate amounts to convert to acetyl-CoA which leads to the fatty acid and arachidonic acid synthesis. In summary, our findings suggest that the metabolic reprogramming in M1 macrophages promotes efficient citrate utilization to support the inflammatory response.

The increase in glycolysis elevated amounts of glycolytic intermediates promote the pentose phosphate pathway (PPP) (Wculek, Dunphy, Heras-Murillo, Mastrangelo, & Sancho, 2022), and the PPP involved chemicals 2-deoxyribose-5-phosphate and D-ribulose 5-phosphate were detected in our research. D-ribulose 5-phosphate is one of the final products in PPP. It decreased after M0 was polarized to M1 because D-ribulose-5 phosphate is one of the precursor molecules for the synthesis of amino acids and the production of energy.

M1 macrophages typically exhibit low arginase activity. This minimizes the diversion of L-arginine to other metabolic pathways, favoring its utilization by iNOS to produce nitric oxide (NO) (Rath, Müller, Kropf, Closs, & Munder, 2014). We also found that L-arginine levels were higher in our inflammatory Caco-2 and THP-1 direct co-culture model compared to the healthy model, but levels of glutamic acid and aspartic acid were reduced. These two amino acids are involved in L-arginine biosynthesis in mammals (Nüse, Holland, Rauh, Gerlach, & Mattner, 2023), which may imply the involvement of L-arginine biosynthesis to support the high demand for NO production in M1. The different metabolic profiles indicated that inflammation could influence energy metabolism and amino acid metabolism, therefore it is suggested that all chemicals related to possible pathways should be detected, while also the modification of specific enzymes and genes should be verified in the future.

The information on metabolomics in the inflammatory Caco-2 and THP-1 direct co-culture model was provided by comparing their metabolites. The metabolites in the same cluster were diverse in their chemical structures, and some of the metabolites have been proved to influence the inflammatory response and cytokine production in M1 macrophages. In cluster 1 and 2, treatments (CD-HST, NL-HST, and

CGN-CH-NL-HST) had higher amounts of metabolites compared to the digestion control, implying that these compounds may have anti-inflammatory effects. For example, esculetin and glycyrrhetic acid can inhibit the production of pro-inflammatory cytokines and might suppress the activity of macrophages, reducing inflammation (Richard, 2021; Zhang, Xie, & Li, 2022). 5′-S-methylthioadenosine (MTA) is a nucleoside, which was found to reduce the COX-2 expression in LPS-stimulated RAW 264.7 cells (Hevia et al., 2004). MTA amount in CGN-CH-NL-HST treatment was especially higher than digestion control and free HST in cluster 1, thereby possibly being relevant to the low COX-2 expression of CGN-CH-NL-HST in the qPCR result (Fig. 4F). In cluster 2, hesperetin, harpagide, and isosakuranetin were bioactive compounds, potential being antioxidant and anti-inflammatory during LPS-induced inflammation (Hădărugă & Hădărugă, 2023; Xu et al., 2024). Hesperetin and isosakuranetin are flavonoids while harpagide is an iridoid glycoside. They all have many hydroxyl groups on their chemical structure, which can reduce oxidative stress and the ensuing inflammation. This suggested in the encapsulated HST group with higher abundances of these metabolites than the digestion control or free HST could exhibit enhanced anti-inflammatory effects. In cluster 3 and 4, amino acids (proline, tryptophan, L-asparagine, glutamine, L-phenylalanine) are essential for cellular metabolism and protein synthesis, and maybe supporting the metabolic needs of activated macrophages (Kieler, Hofmann, & Schabbauer, 2021; Li et al., 2022; Xu et al., 2021), but the relationship between protein synthesis and macrophages as pro (anti) inflammatory differentiation still needs to be investigated in the future.

In summary, alterations in the metabolic profile of macrophages also correspond to phenotypic differentiation. The metabolomic profile of M1 macrophages in co-culture was quite distinctive after LPS stimulation, including enhanced aerobic glycolysis, PPP pathway activation, and low arginase activity. The metabolic fingerprint of co-cultured M1 macrophages treated with encapsulated HST differed from the digestion group. This difference was exhibited by an increase in flavonoid metabolites related to HST as well as some metabolites with anti-inflammatory activity, showing the therapeutic potential of encapsulated HST for inflammatory bowel disease.

5. Conclusion

In conclusion, a direct Caco-2 and THP-1 co-culture cell model was developed in this study to accurately investigate the effects of encapsulated flavonoids after digestion. The model exhibited a pro-inflammatory phenotype when exposed to LPS, making it a good functional model to study inflammatory intestinal diseases such as IBD. (Anti) Inflammatory effects were investigated using HST as a model compound. HST encapsulated within a carrageenan-chitosan coated nanoliposome (CGN-CH-NL-HST) showed the most effective anti-inflammatory functionality. IL-8 was significantly reduced, important inflammation-related genes were downregulated and the metabolic pathway of the inflammatory Caco-2 and THP-1 co-culture model was altered. These findings suggest that the direct Caco-2 and THP-1 co-culture model can be further used to test the potential of other compounds in the inflammation. Flavonoids can be potential anti-inflammatory compounds in IBD, and CGN-CH-NL delivery system is a promising strategy to improve the functionalities of hydrophobic bioactives.

CRediT authorship contribution statement

Xiangnan Meng: Writing – original draft, Visualization, Validation, Investigation, Formal analysis, Conceptualization. **Monic M.M. Tomassen:** Supervision, Methodology, Investigation. **Christos Fryganas:** Writing – review & editing, Supervision, Methodology, Investigation. **Vincenzo Fogliano:** Writing – review & editing, Supervision, Project administration, Funding acquisition, Conceptualization. **Tamara Hoppenbrouwers:** Writing – review & editing, Supervision, Resources, Project administration, Conceptualization.

Funding

This work was partly financial supported by the program of the China Scholarships Council (No.202006350043).

Declaration of competing interest

The authors declare that they have no known competing financial interests or personal relationships that could have appeared to influence the work reported in this paper.

Acknowledgment

The authors would like to thank Dianne van de Berg-Somhorst for RNA gel electrophoresis training, and Jamie Sy for qPCR training.

Appendix A. Supplementary data

Supplementary data to this article can be found online at https://doi.org/10.1016/j.foodres.2025.115916.

Data availability

Data will be made available on request.

References

Abreu, M. T., Arnold, E. T., Thomas, L. S., Gonsky, R., Zhou, Y., Hu, B., & Arditi, M. (2002). TLR4 and MD-2 expression is regulated by immune-mediated signals in human intestinal epithelial cells. *Journal of Biological Chemistry, 277*(23), 20431–20437. https://doi.org/10.1074/jbc.M110333200

Abuawad, A., Mbadugha, C., Ghaemmaghami, A. M., & Kim, D. H. (2020). Metabolic characterisation of THP-1 macrophage polarisation using LC–MS-based metabolite profiling. *Metabolomics, 16*(3). https://doi.org/10.1007/s11306-020-01656-4

Brodkorb, A., Egger, L., Alminger, M., Alvito, P., Assunção, R., Ballance, S., Bohn, T., Bourlieu-Lacanal, C., Boutrou, R., Carrière, F., Clemente, A., Corredig, M., Dupont, D., Dufour, C., Edwards, C., Golding, M., Karakaya, S., Kirkhus, B., Le Feunteun, S., … Recio, I. (2019). INFOGEST static in vitro simulation of gastrointestinal food digestion. *Nature Protocols, 14*(4), 991–1014. https://doi.org/10.1038/s41596-018-0119-1

Chang, X., Zheng, B., Guo, Y., Chen, Y., Xie, J., Shan, J., Wang, Y., Xue, P., Hu, X., Hu, X., & Yu, Q. (2024). Bound polyphenols in insoluble dietary fiber of navel orange peel modulate LPS-induced intestinal-like co-culture inflammation through CSF2-mediated NF-κB/JAK-STAT pathway. *Food and Function, 15*(11), 5942–5954. https://doi.org/10.1039/d3fo05579e

Chanput, W., Mes, J., Vreeburg, R. A. M., Savelkoul, H. F. J., & Wichers, H. J. (2010). Transcription profiles of LPS-stimulated THP-1 monocytes and macrophages: A tool to study inflammation modulating effects of food-derived compounds. *Food and Function, 1*(3), 254–261. https://doi.org/10.1039/c0fo00113a

Coombes, J. L., & Powrie, F. (2008). Dendritic cells in intestinal immune regulation. *Nature Reviews Immunology, 8*(6), 435–446. https://doi.org/10.1038/nri2335

Fedi, A., Vitale, C., Ponschin, G., Ayehunie, S., Fato, M., & Scaglione, S. (2021). In vitro models replicating the human intestinal epithelium for absorption and metabolism studies: A systematic review. *Journal of Controlled Release, 335*, 247–268. https://doi.org/10.1016/J.JCONREL.2021.05.028

Grimm, M. C., Pavli, P., Doe, W. F., Grimm, S. K. M. C., & F Doe, E. W. (1996). Interleukin 8: Cells of origin in inflammatory bowel disease. *Gut, 38*. http://gut.bmj.com/.

Gu, B. H., Kim, M., & Yun, C. H. (2021). Regulation of gastrointestinal immunity by metabolites. In *Nutrients* (Vol. 13, Issue 1, pp. 1–22). MDPI AG. doi: 10.3390/nu13010167.

Hădărugă, D.-I., & Hădărugă, N.-G. (2023). Flavanones in plants and humans. In *Handbook of food bioactive ingredients* (pp. 1–53). Springer International Publishing. https://doi.org/10.1007/978-3-030-81404-5_6-1.

Hasnat, H., Shompa, S. A., Islam, M. M., Alam, S., Richi, F. T., Emon, N. U., Ashrafi, S., Ahmed, N. U., Chowdhury, M. N. R., Fatema, N., Hossain, M. S., Ghosh, A., & Ahmed, F. (2024). Flavonoids: A treasure house of prospective pharmacological potentials. In *Heliyon* (Vol. 10, Issue 6). Elsevier Ltd. doi: 10.1016/j.heliyon.2024.e27533.

He, W., Qu, T., Yu, Q., Wang, Z., Lv, H., Zhang, J., Zhao, X., & Wang, P. (2013). LPS induces IL-8 expression through TLR4, MyD88, NF-kappaB and MAPK pathways in human dental pulp stem cells. *International Endodontic Journal, 46*(2), 128–136. https://doi.org/10.1111/j.1365-2591.2012.02096.x

Hevia, H., Varela-Rey, M., Corrales, F. J., Berasain, C., Martínez-Chantar, M. L., Latasa, M. U., Lu, S. C., Mato, J. M., García-Trevijano, E. R., & Avila, M. A. (2004). 5′-

Methylthioadenosine modulates the inflammatory response to endotoxin in mice and in rat hepatocytes. *Hepatology, 39*(4), 1088–1098. https://doi.org/10.1002/hep.20154

Hickey, J. W., Becker, W. R., Nevins, S. A., Horning, A., Perez, A. E., Zhu, C., Zhu, B., Wei, B., Chiu, R., Chen, D. C., Cotter, D. L., Esplin, E. D., Weimer, A. K., Caraccio, C., Venkataraaman, V., Schürch, C. M., Black, S., Brbić, M., Cao, K., … Snyder, M. (2023). Organization of the human intestine at single-cell resolution. *Nature, 619*(7970), 572–584. https://doi.org/10.1038/s41586-023-05915-x

Hoppenbrouwers, T., Bastiaan-Net, S., Garssen, J., Pellegrini, N., Willemsen, L. E. M., & Wichers, H. J. (2022). Functional differences between primary monocyte-derived and THP-1 macrophages and their response to LCPUFAs. *PharmaNutrition, 22*. https://doi.org/10.1016/j.phanu.2022.100322

Jiang, K., Ma, X., Guo, S., Zhang, T., Zhao, G., Wu, H., Wang, X., & Deng, G. (2018). Anti-inflammatory effects of rosmarinic acid in lipopolysaccharide-induced mastitis in mice. *Inflammation, 41*(2), 437–448. https://doi.org/10.1007/s10753-017-0700-8

Kieler, M., Hofmann, M., & Schabbauer, G. (2021). More than just protein building blocks: How amino acids and related metabolic pathways fuel macrophage polarization. In *FEBS Journal* (Vol. 288, Issue 12, pp. 3694–3714). Blackwell Publishing Ltd. doi: 10.1111/febs.15715.

Koussounadis, A., Langdon, S. P., Um, I. H., Harrison, D. J., & Smith, V. A. (2015). Relationship between differentially expressed mRNA and mRNA-protein correlations in a xenograft model system. *Scientific Reports, 5*. https://doi.org/10.1038/srep10775

Kumar, A., Yassin, N., Marley, A., Bellato, V., Foppa, C., Pellino, G., Myrelid, P., Millan, M., Gros, B., Avellaneda, N., Catalan-Serra, I., El-Hussuna, A., Cunha Neves, J. A., Roseira, J., Cunha, M. F., Verstockt, B., Bettenworth, D., Mege, D., & Brookes, M. J. (2023). Crossing barriers: The burden of inflammatory bowel disease across Western Europe. *Therapeutic advances in gastroenterology* (Vol. 16). https://doi.org/10.1177/17562848231218615

Lei, F., Zeng, F., Yu, X., Deng, Y., Zhang, Z., Xu, M., Ding, N., Tian, J., & Li, C. (2023). Oral hydrogel nanoemulsion co-delivery system treats inflammatory bowel disease via anti-inflammatory and promoting intestinal mucosa repair. *Journal of Nanobiotechnology, 21*(1). https://doi.org/10.1186/s12951-023-02045-4

Li, M., Yang, Y., Xiong, L., Jiang, P., Wang, J., & Li, C. (2023). Metabolism, metabolites, and macrophages in cancer. In *Journal of Hematology and Oncology* (Vol. 16, Issue 1). BioMed Central Ltd. doi: 10.1186/s13045-023-01478-6.

Li, T., Bai, J., Du, Y., Tan, P., Zheng, T., Chen, Y., Cheng, Y., Cai, T., Huang, M., Fu, W., & Wen, J. (2022). Thiamine pretreatment improves endotoxemia-related liver injury and cholestatic complications by regulating galactose metabolism and inhibiting macrophage activation. *International Immunopharmacology, 108*, Article 108892. https://doi.org/10.1016/J.INTIMP.2022.108892

Liu, C., Chu, D., Kalantar-Zadeh, K., George, J., Young, H. A., & Liu, G. (2021). Cytokines: From clinical significance to quantification. *Advanced Science* (Vol. 8(15)). https://doi.org/10.1002/advs.202004433

Liu, Y. (2024). *Glycosylation of FIP-nha and its biological properties* [Wageningen University]. doi: 10.18174/652205.

Liu, Y., Liang, X., Zou, Y., Peng, Y., McClements, D. J., & Hu, K. (2020). Resveratrol-loaded biopolymer core-shell nanoparticles: Bioavailability and anti-inflammatory effects. *Food and Function, 11*(5), 4014–4025. https://doi.org/10.1039/d0fo00195c

Luzardo-Ocampo, I., Loarca-Piña, G., & Gonzalez de Mejia, E. (2020). Gallic and butyric acids modulated NLRP3 inflammasome markers in a co-culture model of intestinal inflammation. *Food and Chemical Toxicology, 146*, Article 111835. https://doi.org/10.1016/J.FCT.2020.111835

Mariano, A., Li, Y. O., Singh, H., McClements, D. J., & Davidov-Pardo, G. (2024). Encapsulation of orange-derived hesperetin in zein/pectin nanoparticles: Fabrication, characterization, stability, and bioaccessibility. *Food Hydrocolloids, 153*. https://doi.org/10.1016/j.foodhyd.2024.110024

Mendes, L. F., Gaspar, V. M., Conde, T. A., Mano, J. F., & Duarte, I. F. (2019). Flavonoid-mediated immunomodulation of human macrophages involves key metabolites and metabolic pathways. *Scientific Reports, 9*(1). https://doi.org/10.1038/s41598-019-51113-z

Meng, X., Fryganas, C., Fogliano, V., & Hoppenbrouwers, T. (2024). Double-coated nanoliposomes improve the bioavailability of flavanone hesperetin. *Food Hydrocolloids, 151*. https://doi.org/10.1016/j.foodhyd.2024.109872

Moerings, B. G. J., Abbring, S., Tomassen, M. M. M., Schols, H. A., Witkamp, R. F., van Norren, K., Govers, C., van Bergenhenegouwen, J., & Mes, J. J. (2024). Rice-derived arabinoxylan fibers are particle size-dependent inducers of trained immunity in a human macrophage-intestinal epithelial cell co-culture model. *Current Research in Food Science, 8*. https://doi.org/10.1016/j.crfs.2023.100666

Muhammad, T., Ikram, M., Ullah, R., Rehman, S. U., & Kim, M. O. (2019). Hesperetin, a citrus flavonoid, attenuates LPS-induced neuroinflammation, apoptosis and memory impairments by modulating TLR4/NF-κB signaling. *Nutrients, 11*(3). https://doi.org/10.3390/nu11030648

Nüse, B., Holland, T., Rauh, M., Gerlach, R. G., & Mattner, J. (2023). L-arginine metabolism as pivotal interface of mutual host–microbe interactions in the gut. In *Gut Microbes* (Vol. 15, Issue 1). Taylor and Francis Ltd. doi: 10.1080/19490976.2023.2222961.

Oliveira, A., Rodrigues, L. C., Soares da Costa, D., Fernandes, E. M., Reis, R. L., Neves, N. M., Leão, P., & Martins, A. (2024). COX-2 inhibitor delivery system aiming intestinal inflammatory disorders. *Biomaterials Advances, 156*, Article 213712. https://doi.org/10.1016/J.BIOADV.2023.213712

Pang, Z., Zhou, G., Ewald, J., Chang, L., Hacariz, O., Basu, N., & Xia, J. (2022). Using MetaboAnalyst 5.0 for LC–HRMS spectra processing, multi-omics integration and covariate adjustment of global metabolomics data. *Nature Protocols, 17*(8), 1735–1761. https://doi.org/10.1038/s41596-022-00710-w

Paul, M. B., Schlief, M., Daher, H., Braeuning, A., Sieg, H., & Böhmert, L. (2023). A human Caco-2-based co-culture model of the inflamed intestinal mucosa for particle toxicity studies. *In Vitro Models, 2*(1), 43–64. https://doi.org/10.1007/s44164-023-00047-y

Peng, L., Guo, F., Pei, M., Tsao, R., Wang, X., Jiang, L., Sun, Y., & Xiong, H. (2022). Anti-inflammatory effect of lentil hull (Lens culinaris) extract via MAPK/NF-κB signaling pathways and effects of digestive products on intestinal barrier and inflammation in Caco-2 and Raw264.7 co-culture. *Journal of Functional Foods, 92*, Article 105044. https://doi.org/10.1016/J.JFF.2022.105044

Protić-Rosić, I., Lopandić, Z., Popović, D., Blagojević, G., & Gavrović-Jankulović, M. (2024). rBet v 1a-BanLecwt induce upregulation of IL-10 and IFN-γ gene expression in Caco-2/THP-1 co-culture and secretion of IL-10 and IFN-γ/IL-4 levels in PBMCs of birch pollen allergic donors. *International Immunopharmacology, 129*. https://doi.org/10.1016/j.intimp.2024.111607

Ran, X., Hu, G., Guo, W., Li, K., Wang, X., Liu, J., & Fu, S. (2024). Hesperetin regulates the intestinal flora and inhibits the TLR4/NF-κB signaling axis to protect the blood-milk barrier and prevent mastitis. *Life Sciences, 342*, Article 122533. https://doi.org/10.1016/J.LFS.2024.122533

Rath, M., Müller, I., Kropf, P., Closs, E. I., & Munder, M. (2014). Metabolism via arginase or nitric oxide synthase: Two competing arginine pathways in macrophages. In *Frontiers in immunology* (Vol. 5, Issue OCT). Frontiers Media S.A. doi: 10.3389/fimmu.2014.00532.

Richard, S. A. (2021). Exploring the pivotal immunomodulatory and anti-inflammatory potentials of glycyrrhizic and glycyrrhetinic acids. In *Mediators of inflammation* (Vol. 2021). Hindawi Limited. doi: 10.1155/2021/6699560.

Roh, T. T., Chen, Y., Rudolph, S., Gee, M., & Kaplan, D. L. (2021). In vitro models of intestine innate immunity. In *Trends in biotechnology* (Vol. 39, Issue 3, pp. 274–285). Elsevier Ltd. doi: 10.1016/j.tibtech.2020.07.009.

Sarker, N., Fabijan, J., Emes, R. D., Hemmatzadeh, F., Meers, J., Moreton, J., Owen, H., Seddon, J. M., Simmons, G., Speight, N., Trott, D., Woolford, L., & Tarlinton, R. E. (2018). Identification of stable reference genes for quantitative PCR in koalas. *Scientific Reports, 8*(1). https://doi.org/10.1038/s41598-018-21723-0

Shishir, M. R. I., Karim, N., Gowd, V., Xie, J., Zheng, X., & Chen, W. (2019). Pectin-chitosan conjugated nanoliposome as a promising delivery system for neohesperidin: Characterization, release behavior, cellular uptake, and antioxidant property. *Food Hydrocolloids, 95*, 432–444. https://doi.org/10.1016/J.FOODHYD.2019.04.059

Soares, J. B., Pimentel-Nunes, P., Roncon-Albuquerque, R., & Leite-Moreira, A. (2010). The role of lipopolysaccharide/toll-like receptor 4 signaling in chronic liver diseases. *Hepatology International, 4*(4), 659–672. https://doi.org/10.1007/s12072-010-9219-x

Tucureanu, M. M., Rebleanu, D., Constantinescu, C. A., Deleanu, M., Voicu, G., Butoi, E., Calin, M., & Manduteanu, I. (2018). Lipopolysaccharide-induced inflammation in monocytes/macrophages is blocked by liposomal delivery of Gi-protein inhibitor. *International Journal of Nanomedicine, 13*, 63–76. https://doi.org/10.2147/IJN.S150918

Vreeburg, R. A. M., Bastiaan-Net, S., & Mes, J. J. (2011). Normalization genes for quantitative RT-PCR in differentiated Caco-2 cells used for food exposure studies. *Food and Function, 2*(2), 124–129. https://doi.org/10.1039/c0fo00068j

Wculek, S. K., Dunphy, G., Heras-Murillo, I., Mastrangelo, A., & Sancho, D. (2022). Metabolism of tissue macrophages in homeostasis and pathology. In *Cellular and Molecular Immunology* (Vol. 19, Issue 3, pp. 384–408). Springer Nature. Doi: 10.1038/s41423-021-00791-9.

Xu, C., Tang, Y., Yang, H., Jiang, S., Peng, W., & Xie, R. (2024). Harpagide inhibits the TNF-α-induced inflammatory response in rat articular chondrocytes by the glycolytic pathways for alleviating osteoarthritis. *International Immunopharmacology, 127*, Article 111406. https://doi.org/10.1016/J.INTIMP.2023.111406

Xu, Y., Shi, T., Cui, X., Yan, L., Wang, Q., Xu, X., Zhao, Q., Xu, X., Tang, Q., Tang, H., & Pan, D. (2021). Asparagine reinforces mTORC1 signaling to boost thermogenesis and glycolysis in adipose tissues. *The EMBO Journal, 40*(24). https://doi.org/10.15252/embj.2021108069

Yokoyama, T., Komori, A., Nakamura, M., Takii, Y., Kamihira, T., Shimoda, S., Mori, T., Fujiwara, S., Koyabu, M., Taniguchi, K., Fujioka, H., Migita, K., Yatsuhashi, H., & Ishibashi, H. (2006). Human intrahepatic biliary epithelial cells function in innate immunity by producing IL-6 and IL-8 via the TLR4-NF-κB and -MAPK signaling pathways. *Liver International, 26*(4), 467–476. https://doi.org/10.1111/j.1478-3231.2006.01254.x

Zhang, L., Xie, Q., & Li, X. (2022). Esculetin: A review of its pharmacology and pharmacokinetics. In *Phytotherapy Research* (Vol. 36, Issue 1, pp. 279–298). John Wiley and Sons Ltd. Doi: 10.1002/ptr.7311.